Applied Catalysis O: Open 208 (2025) 207073

Contents lists available at ScienceDirect

Applied Catalysis O: Open

journal homepage: www.elsevier.com/locate/apcato

An innovative approach to evidence pathways in a reactional mechanism of heterogenous catalysis

Tristan Cabanis [a], Aline Auroux [a], Jean-Luc Dubois [b], Nicolas Sbirrazzuoli [c,*], Georgeta Postole [a,*]

[a] Universite Claude Bernard Lyon 1, CNRS, IRCELYON, UMR 5256, Villeurbanne F-69100, France
[b] Trinseo Netherlands B.V., Innovatieweg 14, 4542 NH Hoek, the Netherlands
[c] Institut de Chimie de Nice (ICN) – UMR CNRS 7272, Université Côte d'Azur (UCA), 28 avenue Valrose, 06108 Nice, Cedex 2, France

ARTICLE INFO

Keywords:
Pulse catalytic test set up inside a calorimeter
Isopropanol conversion
Propylene
Alumina
Kinetics

ABSTRACT

In this study, a pulse catalytic test set inside a microcalorimeter has been developed for studying the different steps of the heterogeneous catalytic mechanism of isopropanol dehydration to propylene. Adsorption of reactants and desorption of products are studied from an energetic point of view at temperatures in the range of 125 to 250 °C, and over commercial alumina catalyst.

Results are discussed in terms of heats of adsorption, reaction and desorption of the gaseous reagent and products on the active sites of the catalyst surface. Isopropanol conversion and kinetic analysis of calorimetric signals are investigated. Heat flow signals were analyzed both at low temperature (125 °C) when only adsorption/desorption occurs, and at high temperature (>175 °C) with occurrence of adsorption, reaction and desorption.

Strong dissociative adsorption was refuted from the different process steps. Meaningful kinetic parameters gave insight into the limiting steps and the reaction mechanism by analyzing the exothermic and endothermic contribution separately. Two models were used to fit the calorimetric signals, and two possible surface mechanisms are discussed: the second order elimination (E2) and the first order elimination through a carbanion path (E1cb).

1. Introduction

The interaction at the catalyst surface is the key for understanding the fundamental mechanisms in heterogenous catalysis taking a vital role in numerous industrial processes [1,2]. The ex-situ characterization of solids is now well established and provides useful information on the structure-reactivity relationships of fresh catalysts (i.e. have not yet been involved in a reaction) and deactivated catalysts. Structural X-ray diffraction, textural nitrogen sorption characterization, electron microscopy and chemical analysis are some techniques commonly present in published literature as they contribute to correlating the catalyst characteristics to the activity. Conventional catalysis research frequently relies on pre- and post-reaction catalyst analysis and kinetic studies while varying parameters.

These conventional characterizations, however, are performed in very different conditions when compared to the heterogeneous reaction environments. Indeed, most characterization techniques operate under drastically different pressure, temperature, and molecular density of reagents and products. These various operating conditions can lead to significant variations in catalyst surface behavior and active site nature.

Consequently, the absence of direct observation in reaction conditions can lead to a variety of interpretations within the same catalytic reaction preventing further data extrapolation. This is the case for alcohols dehydration on alumina catalysts, where extensive work by Knözinger [3–5] followed by several authors such as DeCanio et al. [6], Ouqour et al. [7] and Gervasini et al. [8] show that the nature of the reaction mechanism, i.e. E1, E2, or E1cb (Fig. S1) can easily switch from one to the other when a small change in the operating conditions or surface nature occurs.

However, the technical evolution of instrumentation permitted to improve the scale of structural characterization, but also to apply these measurements under controlled environment, closer to heterogenous catalysis conditions [9]. The term in-situ, although it still has varying interpretations, is used to describe these experiments. When the

* Corresponding authors.
E-mail addresses: Nicolas.SBIRRAZZUOLI@univ-cotedazur.fr (N. Sbirrazzuoli), georgeta.postole@ircelyon.univ-lyon1.fr (G. Postole).

https://doi.org/10.1016/j.apcato.2025.207073
Received 29 July 2025; Received in revised form 2 September 2025; Accepted 9 September 2025
Available online 10 September 2025

apparatus allows catalyst characterization under full processing conditions, the term in-situ, on-line, or *operando*, is used [10]. So-called in-situ and *operando* techniques are now well developed for the study of surfaces and catalytic reactions under more accurate operating conditions. The coupling of catalytic tests with methods such as Fourier transform infrared [11,12], Raman [13,14], and X-ray spectroscopy [15], are some examples of the few developed techniques for direct studies close to industrial reaction conditions. Spectroscopic studies give crucial qualitative structural information about active sites nature and behavior during the catalytic reaction.

Transient techniques are also powerful tools to study catalytic reactions. Temporal Analysis of Products (TAP) and Steady-State Isotopic Transient Kinetic Analysis (SSITKA) techniques, allow for mechanistic and kinetic studies on reactions occurring on the catalyst surface. TAP is a pulse-response technique used to study catalytic reactions by sending small amounts of reactants into a reactor and monitoring the product response over time. This technique is based on high temporal resolution and is useful for uncovering reaction mechanisms, kinetics, and the nature of active sites [16]. However, TAP operates under conditions that do not reflect industrial conditions. SSITKA technique, on the other hand, is based on the rapid replacement of one compound with its isotope while the catalyst operates under a steady state. The SSITKA technique generally allows to determine the number and the surface residence time of intermediates under realistic conditions compared to TAP [17–19]. Further computations can be used to determine kinetic parameters, but these are dependent on assumptions and models regarding the reactor configuration [19].

Thermal analysis and calorimetry are powerful tools for catalyst characterization, and especially when using the adsorption of gas or liquid probe reagents on the solid catalyst surface [20]. Two techniques of adsorption studies are distinguished: static volumetric chemisorption and dynamic (or flow) chemisorption [2].

Static chemisorption microcalorimetry consists of a volumetric apparatus combined with a microcalorimeter. This apparatus has been used to quantify surface site strengths and distribution through interactions with probe molecules and allows sites strength and a number of direct correlations with the catalytic efficiency of a solid. Examples from the literature are abundant. Ammonia (NH_3), sulphur dioxide (SO_2), pyridine and carbon monoxide, for example, were used to characterize the acid-base sites of catalysts [21].

These techniques, however, operate in conditions far from industrial processes, meaning pure gas, no flow and very low pressure. These parameters can radically be far from the adsorption behavior of a catalyst.

Dynamic chemisorption microcalorimetry, on the other hand, operates at constant and controlled gas flow and pressure, breaking the gap between ex situ and in situ or *operando* characterization. Moreover, the temperature, a key parameter in all adsorption and reaction processes, can be well controlled in such system. Such techniques may rely on successive injections of precise quantity of a probe molecule until sample saturation. A calibrated thermal conductivity detector (TCD) monitors the amount of non-adsorbed probes, allowing for calculating the adsorbed amount from a blank experiment [2]. Brown and Groszek [22] and Felix et al. [23] have applied pulse flow microcalorimetry to characterize solid acid catalysts, conducting a comparative study of the static and dynamic method and discussing the kinetic and thermodynamic control of the pulse flow microcalorimetry technique. Yuan et al. [24] recently used flow-pulse adsorption microcalorimetry to determine differential heats of ammonia adsorption on various zeolites. You et al. [25] have used the coupling of a Tian-Calvet microcalorimeter and a chemisorption apparatus to determine the heat flow and adsorbed amount of CO on cerium oxide and palladium/cerium oxide powders at −50 and – 100 °C. Lebars et al. [26], using the same kind of apparatus, experienced conditions such that the “probe” molecule gets converted after adsorption (e.g. ethane to ethylene on vanadium oxide and γ-alumina). Through these considerations, they were able to determine the global enthalpy of reaction. Lin et al. [27] also applied in situ pulse calorimetry to evaluate CO oxidation heats.

While the integrated value of heat flow signals is linked to endothermic or exothermic heat, the thermal analysis signals as a function of time and temperature can be correlated to the kinetics of the effect being observed. Heat flow signal computations have already been used to determine the kinetic parameters of several solid-state reactions [28,29]. For example, Friedman [30] studied the kinetics of thermal degradation of phenolic plastics using thermogravimetric data, while Vyazovkin and Sbirrazzuoli used the advanced isoconversional method on non-isothermal calorimetry data to determine the activation energy of polyethylene terephthalate crystallization [31] and the mechanism of epoxy-amine cure [32].

Knowing how kinetics are important in catalysis research, applying those methods to a thermal event linked to a catalytic reaction would provide interesting information for the field.

Most kinetic studies in catalysis are based on Arrhenius plot and requires a low conversion, or low differential/incremental conversion, to simultaneously minimize the influence of equilibrium, avoid a significant change in temperature if the reaction is endothermic or exothermic, and ensure a constant concentration of reagents and products along the reactor for uniform catalyst utilization. Therefore, fundamental kinetic studies are done at very low contact time and very high linear velocity compared to industrial processes, to eliminate heat and mass transfer limitations. The kinetic methods employed in this study differ slightly from kinetic analysis performed at low conversion relying on Arrhenius plot and have demonstrated their efficiency in numerous applications [28,29,31–33]. In this work it is shown that these methods can also provide reliable evaluations of kinetic parameters and yield new insights into reaction mechanisms within the field of catalysis.

An experimental setup was built to measure the heat flow signals involved during the catalytic dehydration of isopropanol to propylene. A pulse catalytic test is located inside a Calvet-type calorimeter and directly linked to a gas chromatography (GC) apparatus. The Calvet-type calorimeter has the advantage of offering a geometry similar to a tubular reactor. This coupling enables the differential heats of the catalytic process to be directly measured including adsorption, desorption, and reaction and was used to study the catalytic conversion of isopropanol. This system allows also to estimate the reaction time between adsorption and desorption.

Catalytic conversion of isopropanol (IPA) is used as it is a well-known reaction in laboratories, especially to determine the acid-base properties of a catalyst. Acidic surface sites trigger the dehydration, and yield propylene (PEN) (Eq. 1) or diisopropyl ether (DIPE) (Eq. 2) through respectively an endothermic and an exothermic reaction, while basic surface sites trigger the dehydrogenation and yield acetone (ACE) and hydrogen through an endothermic reaction (Eq. 3) [8,34].

$$C_3H_8O_{(g)} \rightarrow C_3H_{6(g)} + H_2O_{(g)} \quad \Delta_r H^0_{298\,K,1\,atm} = +51.0\ kJ{\cdot}mol^{-1} \tag{1}$$

$$2\,C_3H_8O_{(g)} \rightarrow C_6H_{14}O_{(g)} + H_2O_{(g)} \quad \Delta_r H^0_{298\,K,1\,atm} = -15.0\ kJ{\cdot}mol^{-1} \tag{2}$$

$$C_3H_8O_{(g)} \rightarrow C_3H_6O_{(g)} + H_{2(g)} \quad \Delta_r H^0_{298\,K,1\,atm} = +55.7\ kJ{\cdot}mol^{-1} \tag{3}$$

Moreover, dehydration of isopropanol into propylene is a hot topic in the scientific and industrial community. Indeed, isopropanol is one of the bio-alcohols that can result from biomass or carbon dioxide (CO_2) conversion, which aligns with current efforts to establish sustainable carbon cycles. It is produced from acetone which is a coproduct of the cumene oxidation process to phenol. The conversion of acetone into isopropanol, then into propylene, is of great interest for closing the C_3 loop and saving carbon [35].

2. Experimental

2.1. Catalyst

The catalyst studied is a commercially available alumina (Al_2O_3) catalyst as supplied by Grace (DAVICAT® 2772). The catalyst was received shaped, therefore it was crushed and sieved to different particle sizes depending on the technical requirements.

2.2. X-ray diffraction

The X-ray diffraction (XRD) pattern of the commercial powder was recorded on a Brüker D8 Advance powder diffractometer with monochromatic Cu Kα radiation of 1.5406 Å wavelength, equipped with a 1-D fast multistrip detector (LynxEye, 192 channels, 2.95°) and a Ni filter. The diffractogram, registered within the 2θ range from 4 to 80° with a 0.02° step size, was analyzed using the Diffract Eva software and the PDF4+ database.

2.3. Nitrogen sorption isotherm

Nitrogen (N_2) sorption isotherms were recorded at −196 °C on an ASAP 2010 (Micromeritics) apparatus. The sample was first outgassed under secondary vacuum for 3 h at 300 °C. The apparent specific surface area (S_{BET}) was derived from the Brunauer-Emmett-Teller (BET) standard equation. The interval of relative pressure used to linearize the BET model equation was $0.005 \leq P/P_0 \leq 0.10$ with at least 5 points used to obtain a correlation coefficient > 0.999. The total pore volume (V_{tot}) was calculated at $P/P_0 = 0.98$ on the adsorption branch. The mesopore size distribution was determined by analyzing the adsorption branch of the N_2 adsorption/desorption isotherm (BJH method).

2.4. Acid-base microcalorimetry

The acid/base properties of the Al_2O_3 sample were determined at 150 °C by adsorption microcalorimetry of NH_3 and SO_2 probe molecules, respectively. The adsorption experiments were performed in a heat flow microcalorimeter (Tian-Calvet type, C80 from Setaram) linked to a conventional volumetric apparatus and equipped with a Barocel capacitance manometer (Datametrics) for pressure measurements. Prior to the SO_2 or NH_3 adsorption, about 0.100 g of the sample was treated overnight at 400 °C (1 °C · min^{-1}) under vacuum. The differential heats of adsorption were measured as a function of coverage by repeatedly sending small doses of probe molecules over the powder until an equilibrium pressure of about 67 Pa was reached. The sample was then outgassed for 30 min at the same temperature and a second adsorption was performed (still at 150 °C) until an equilibrium pressure of about 27 Pa was attained to calculate the amount of irreversible adsorption at this pressure. The difference between the amounts of gas adsorbed at 27 Pa during the two adsorption runs corresponds to the number of strong adsorption sites.

2.5. Fourier transform infra-red ammonia adsorption

FTIR spectra were recorded at a resolution of 4 cm^{-1} in the region of 1000 to 4000 cm^{-1} by using a Thermo Scientific (Waltham, MA, USA) Nicolet 8700 Fourier transform spectrometer equipped with a DTGS detector and OMNIC software. Prior to analysis, approximately 30 to 40 mg of sample was grounded in an agate mortar and pressed into self-supporting discs by applying 5 tons pressure. The self-supported wafer was placed into a cell with CaF_2 windows and activated under oxygen overnight at 400 °C (1 °C·min^{-1}), followed by 2 h outgassing at the same temperature before adsorption. Then, the cell was cooled down to 23 °C, and the sample was contacted with NH_3 (15 mbars) for 1 h before following the desorption of the adsorbed species, under vacuum, at 25, 100, 200, 300 and 400 °C, respectively. The IR spectra were recorded after each step: pretreatment, adsorption and desorption at these temperatures.

2.6. Pulse differential scanning calorimetry – Gaz chromatography

Pulse experiments were carried out in a quartz microreactor placed in a differential scanning calorimeter (DSC) (CALVET PRO from Setaram) connected to a gas chromatograph (GC) as shown in Fig. 1.

The reaction cells are 6.35 mm in diameter quartz tubes fitting perfectly into the Calvet-type DSC in such a way that direct contact is made between the DSC and reactor external walls. Typically, 15 mg of catalysts with particle sizes of 300 to 425 μm are loaded on a sintered silica glass frit in the DSC isothermal zone. The catalyst is constantly flushed with a 30 mL · min^{-1} helium flow.

A saturator filled with isopropanol and maintained at a constant temperature of 30.5 °C is constantly fed by a helium flow of 30 mL · min^{-1}. This feed system is connected to a 6-port valve set in the GC oven. The valve is equipped with a calibrated injection loop with a defined volume. This system enables continuous delivery of the IPA quantities in the injection loop. In the saturator, isopropanol is supposed to be at liquid/gas equilibrium. Antoine's equations are used to calculate the partial pressure of IPA in the flow feeding the injection loop.

Blank experiments at different temperatures flow rates and IPA volumes in the saturator were carried out to verify the equilibrium state in the saturator. Since the IPA peak areas in the chromatograph's detectors remain independent of helium flow rate and IPA volume in the saturator, and are uniquely related to temperature by Antoine's equation, the assumption is verified.

The outlet of the microreactor is directly connected to a Porapak Q column and to thermal conductivity (TCD) and flame ionization (FID) detectors placed in series. The column is the main source of pressure drop, generating a pressure of 3 bars inside the reactor.

The feed gas mixture is composed of 8 mol% of isopropanol in helium. The loop volume is 500 μL. The amount of isopropanol per injection is then 1.15 μmol. Detailed calculations are available in the ESI. To prevent condensation of liquid reagents and products at room temperature, all lines connecting the saturator, chromatograph and reactor are heated to 110 °C.

A pretreatment step is done at the maximum study temperature (300 °C) for 90 min under a pure helium flow (30 mL · min^{-1}) prior to any injection.

As injections start, the 6-port valve is switched to direct the reagent and carrier gas flow (8 % IPA/He, 30 mL · min^{-1}) to the microreactor.

Calorimetric curves display any heat signal (exotherm and/or endotherm) during the pulse, while FID chromatograms are used for quantification of reagents and products and TCD results for qualitative observation of water peaks. The interval between each pulse lasts 90 min. This relatively long duration is necessary for the heat flux and GC detector signals to return to the baseline.

The first pulses were performed at 125 °C as no reaction, but only adsorption/desorption occurs at such a low temperature. When no more significant change in the calorimetric curve or chromatogram was observed compared to previous pulses, maximum catalyst surface coverage by the probe reagent was assumed. Then, the DSC temperature was increased to reaction temperature. A given number of injections (typically 6) were always performed to ensure reproducibility.

The GC is calibrated using an empty reactor set at 110 °C (same temperature as the heated lines). For liquid reagent (IPA) and products (ACE and DIPE), the temperature of the saturator was varied, and different loop volumes were used for each fixed temperature. For the gas product (PEN), calibration was made by changing the loop volumes. From those calibrations, the response factor of each compound was determined. The adsorbed and reacted amount of isopropanol n_{ads}^{IPA} (mol) was calculated as follows (Eq. 4):

$$n_{ads}^{IPA} = n_{in}^{IPA} - n_{out}^{IPA} \quad (4)$$

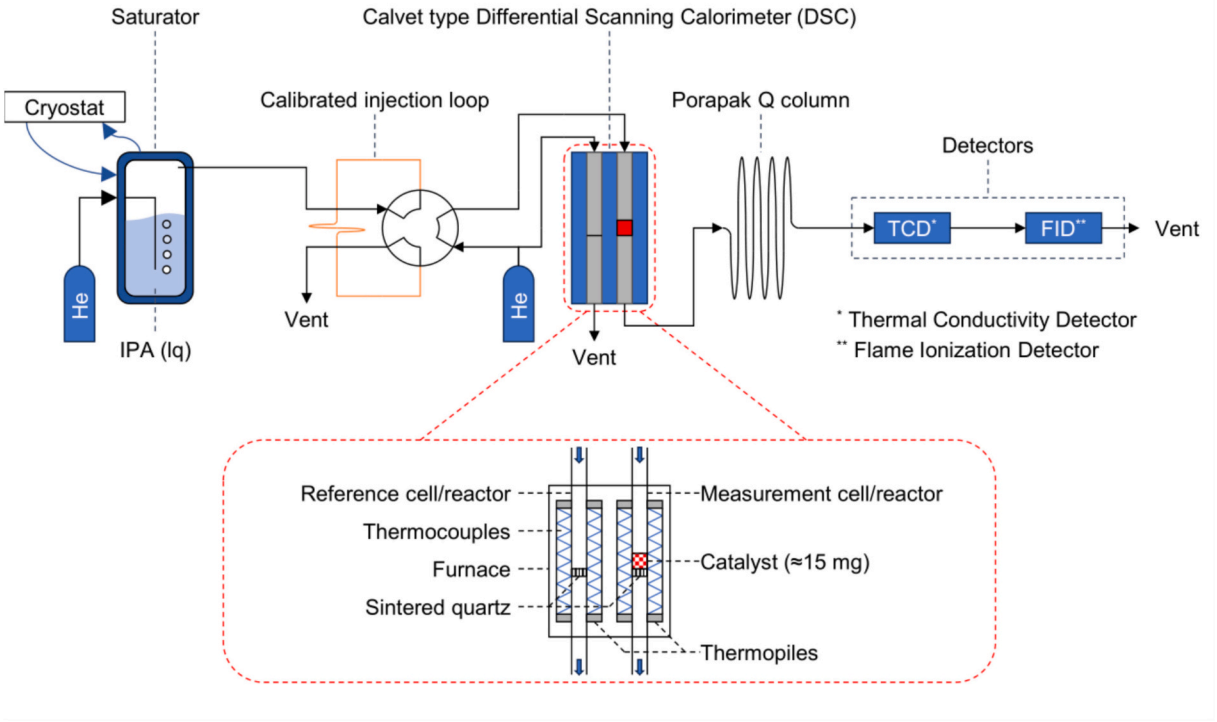

Fig. 1. DSC – GC coupling.

with n_{in}^{IPA}, the amounts of isopropanol injected per dose, e.g. 1.15 μmol, and n_{out}^{IPA} the amounts of isopropanol detected at the reactor outlet.

The deconvolution of the calorimetric curves was performed using an in-house Python program. The Fraser-Suzuki function (Eq. 5), frequently used for deconvolution of kinetic data [36,37], coupled with the least squares method, was used to deconvolute the exothermic peak of adsorption and the endothermic peak of reaction/desorption.

$$y = a_0 \exp\left[-\ln 2\left[\frac{\ln\left(1+2a_3\frac{x-a_1}{a_2}\right)}{a_3}\right]^2\right] \quad (5)$$

where a_0, a_1, a_2 and a_3 are respectively the amplitude, position, half-width and asymmetry of the peak. The integrated area of the peaks was directly determined from deconvoluted results.

Differential heats $Q_{diff}\left(\text{kJ·mol}^{-1}\right)$ of adsorption were calculated as follows (Eq. 6):

$$Q_{diff} = \frac{-E}{n_{ads}^{IPA}} \quad (6)$$

where E (J) is the integrated energy and n_{ads}^{IPA} (mol) is the total amount of isopropanol adsorbed/reacted for each pulse.

2.7. Kinetic computation

One important parameter for kinetic analysis is the extent of conversion, α. This parameter can easily be computed from calorimetric data by dividing the integrated heat flow at time t (Q_t) by the total measured heat release by the reaction (Q_{Tot}) (i.e. the energy released divided by the amounts of reactant adsorbed or converted) (Eq. 7):

$$\alpha = \frac{\int_{t_i}^{t}(dQ/dt)\,dt}{\int_{t_i}^{t_f}(dQ/dt)\,dt} = \frac{Q_t}{Q_{Tot}} \quad (7)$$

where t is the time, (dQ/dt) is the heat flow, t_i and t_f represent respectively the time of the first and last integration limits of the calorimetric signal. Then, the reaction rate $(d\alpha/dt)$ is obtained according to (Eq. 8):

$$\frac{d\alpha}{dt} = \left(\frac{dQ}{dt}\right)\Big/ Q_{Tot} \quad (8)$$

The basic rate equation used in kinetic analysis of condensed phase processes is typically expressed as (Eq. 9) [33]:

$$\frac{d\alpha}{dt} = k(T)f(\alpha) \quad (9)$$

where T is the absolute temperature, $k(T)$ is the rate coefficient, the function $f(\alpha)$ is the differential form of the mathematical function describing the reaction model related to the reaction mechanism. Introducing the Arrhenius equation for the rate coefficient, leads to (Eq. 10):

$$\frac{d\alpha}{dt} = A\exp\left(-\frac{E_a}{RT}\right)f(\alpha) \quad (10)$$

where E_a is the activation energy and A the pre-exponential factor.

Advanced isoconversional kinetic methods have been applied with success in the recent years to describe a wide range of physicochemical transformations and have been used in this study [38]. The most used and reliable isoconversional methods are the Friedman's and the Vyazovkin's methods [28,29,39]. These methods were implemented in a self-designed software and used in this study [40–43]. In contrast with classical model-fitting methods, such methods give what is called the effective or apparent activation energy E_α as a function of the extent of conversion or temperature. Because the computations are done for constant values of α, it can be demonstrated that the E_α values are determined without any assumption on the mathematical function that describes the reaction mechanism, $f(\alpha)$. If constant values of E_α are obtained through the whole process, it is concluded that the reaction obeys a single-step process. In contrast, the variation of E_α with the

extent of conversion indicates that the reaction mechanism is complex, i.e. it follows a multi-step process. In addition, analysis of these variations gives information on the reaction mechanism and may help with its elucidation. The values of the logarithm of the pre-exponential factor ($\ln(A_\alpha)$) and of the mathematical function $f(\alpha)$ that represents the reaction mechanism were also computed in a model-free way using the method already described and using the compensation effect (CE) to estimate $\ln(A_\alpha)$ [28,42–44]. This method based on the Vyazovkin's algorithm is named NLN in the self-designed software used.

3. Results and discussion

3.1. Ex situ characterization

Fig. 2 shows the XRD pattern, nitrogen adsorption-desorption isotherm and pore size distribution of the studied alumina. The XRD peak positions (2θ = 31.6°, 32.8°, 37.1°, 39.9°, 45.3°, 50.9°, 60.1° and 67.5°) correspond to theta phase with the monoclinic crystal system [45]. The N_2 adsorption–desorption isotherm is of type IV (IUPAC classification) presenting an increased nitrogen uptake at $P/P_0 < 0.6$ and an H1 type hysteresis loop characteristic of mesoporous structures [46]. The sample displays a BET surface area of 117 $m^2 \cdot g^{-1}$ and a mesoporous pore volume of 0.57 $m^2 \cdot g^{-1}$, which represents 96 % of the total pore volume (0.60 $m^2 \cdot g^{-1}$). The average pore width calculated using $4V/A$ by BET adsorption is 20.5 nm with a peak maximum at 13.1 nm.

De Boer and Lippens [47] used the hysteresis loops of adsorption and desorption isotherms to describe the shape of the pores. The obtained nitrogen sorption curve shows a type B hysteresis loop, i.e. very wide pores with narrow openings or slit-shaped pores, characteristic of aggregates of plate-like particles.

Fig. 3 displays the differential heats of adsorption of NH_3 (right-hand side) and SO_2 (left-hand side) as a function of surface coverage, thus featuring the acid and basic sites on the catalyst surface at 150 °C. The θ-alumina appears to be amphoteric. Indeed, both SO_2 and NH_3 are significantly adsorbed on the alumina surface. The irreversible and reversible volumes at 27 Pa and 150 °C are respectively 200 and 25 µmol $\cdot g^{-1}$ for SO_2 and 157 and 97 µmol $\cdot g^{-1}$ for NH_3.

The alumina surface coverage by the chemisorbed probes corresponds to 4.3 % for NH_3 and 15.5 % for SO_2 respectively, and thus a total coverage of approximately 20 %.

For basic sites, i.e. SO_2 uptake, Fig. 3 (b) reveals a slight differential heat decrease (in absolute value) from −174 to −103 kJ $\cdot$ mol^{-1} up to the 200 µmol $\cdot g^{-1}$ coverage corresponding to the irreversible uptake before a drastic drop to −34 kJ $\cdot$ mol^{-1} in the physisorption field. For acid sites, i.e. NH_3 uptake, the differential heat curve decelerates quickly from −200 to −53 kJ $\cdot$ mol^{-1} before stabilizing around −32 kJ $\cdot$ mol^{-1} in the physisorption domain.

Such evolution of the differential heat with coverage testify to a wide distribution of acidic and basic sites [48]. Note that the latent heat of liquefaction of NH_3 and SO_2, at 150 °C, are respectively −24 and − 25 kJ $\cdot$ mol^{-1} [49,50]. This acid/base surface study will allow a better understanding of the isopropanol reactivity in the following paragraphs. It is worth mentioning that both acidic and basic surface sites of Al_2O_3 are assumed to adsorb isopropanol, an amphoteric molecule capable of both receiving and donating protons. This characteristic is specific to alcohols and has been demonstrated in previous studies [51].

Fig. 4 displays the FT-IR spectra of theta-alumina and subsequent ammonia adsorption in the stretching (a) and bending (b) domains. Pure theta-alumina shows adsorption bands at 3791, 3770, 3726, 3678, and 3578 cm^{-1}. According to the literature, these bands are associated with OH surface groups and depend on the hapticity of the oxygen atom, i.e., the number of aluminium atoms to which it is bonded [52,53]. After ammonia adsorption, several spectral changes are observed. The bands at 3555, 3494, 3406, 3362, 3272, and 3177 cm^{-1} are attributed to N—H stretching vibrations [54–56]. The hypsochromic shift of the bands at 3726 and 3678 cm^{-1} towards wavenumbers of 3730 and 3685 cm^{-1} respectively, and their decrease in intensity compared to the clean surface indicate the presence of interaction between the adsorbed ammonia and surface hydroxides.

The disappearing of the band at 3770 cm^{-1} also supports this conclusion. In the structural frequency range, the band at 1615 cm^{-1} is attributed to the fundamental NH_2 or NH_3 deformation [54]. The additional bands observed at 1183 and 1224 cm^{-1} are assigned to coordinated ammonia on Lewis acid sites. Finally, the weak band observed at 1400 cm^{-1} is associated with NH_4^+ species and supports the presence of Brønsted acid sites on the alumina sample [55].

The band at 1391 cm^{-1} disappears while the bands at 1615 cm^{-1} remain present when the temperature is increased to 200 °C.

The results support the predominance of Lewis acid sites compared to Brønsted at reaction temperatures. Moreover, the surface hydroxide groups are likely to play a role in the adsorption process by hydrogen bonding.

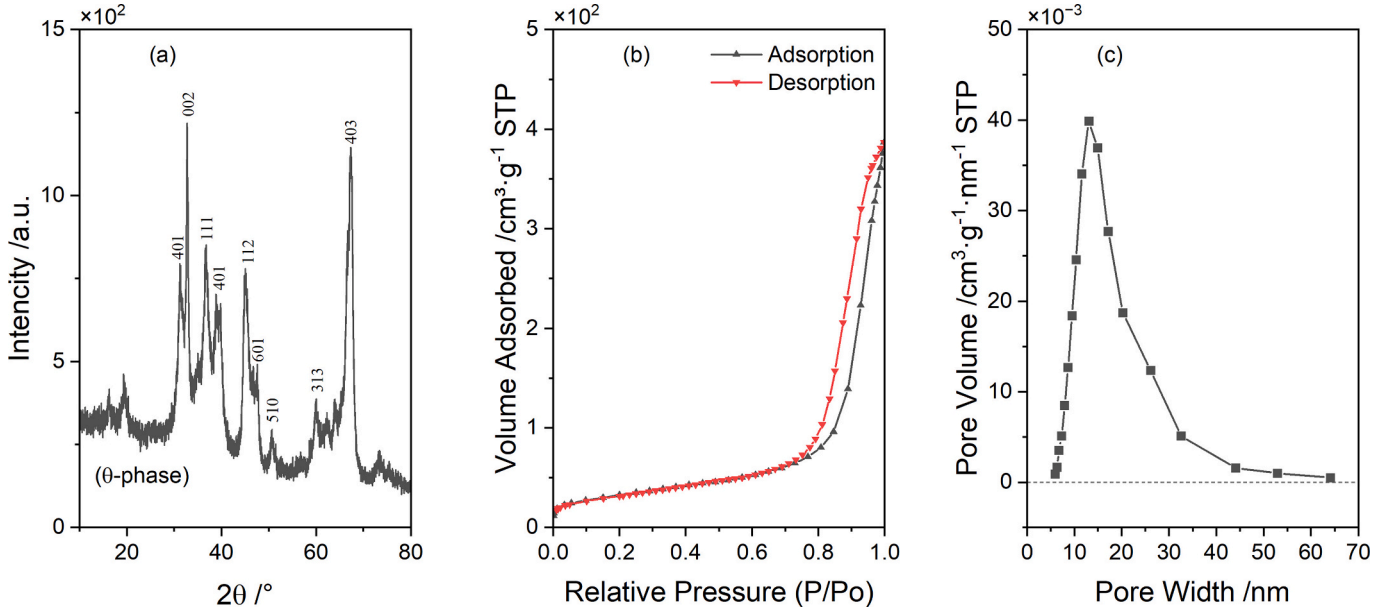

Fig. 2. (a) XRD patterns, (b) N_2 adsorption-desorption isotherm, (c) Pore size distribution obtained through the BJH method for the Al_2O_3 sample.

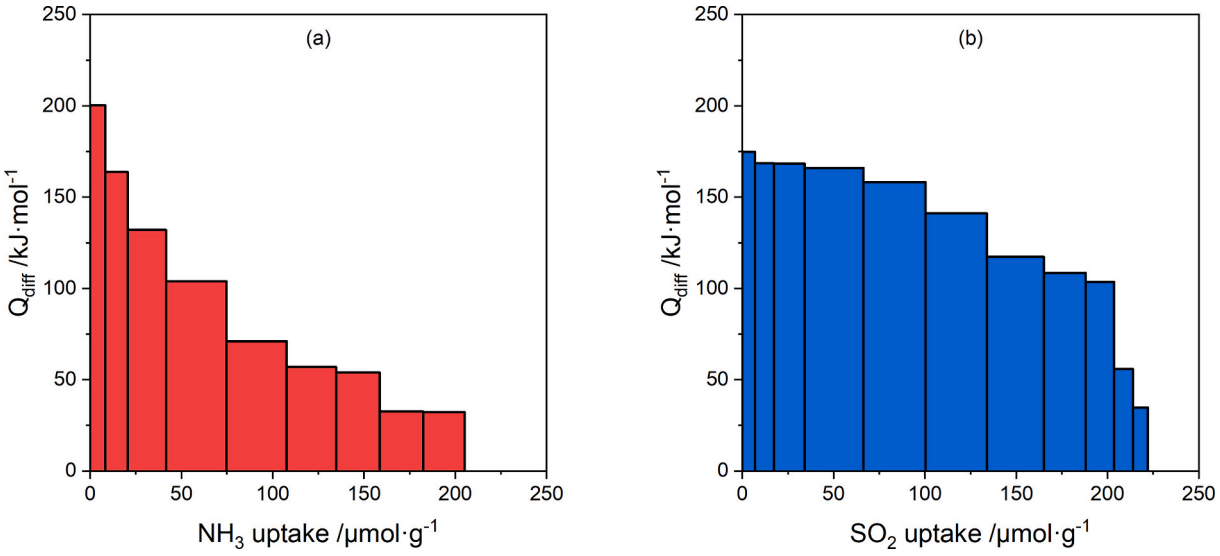

Fig. 3. Differential heats of NH_3 (a) and SO_2 (b) adsorption on Al_2O_3 catalyst at 150 °C.

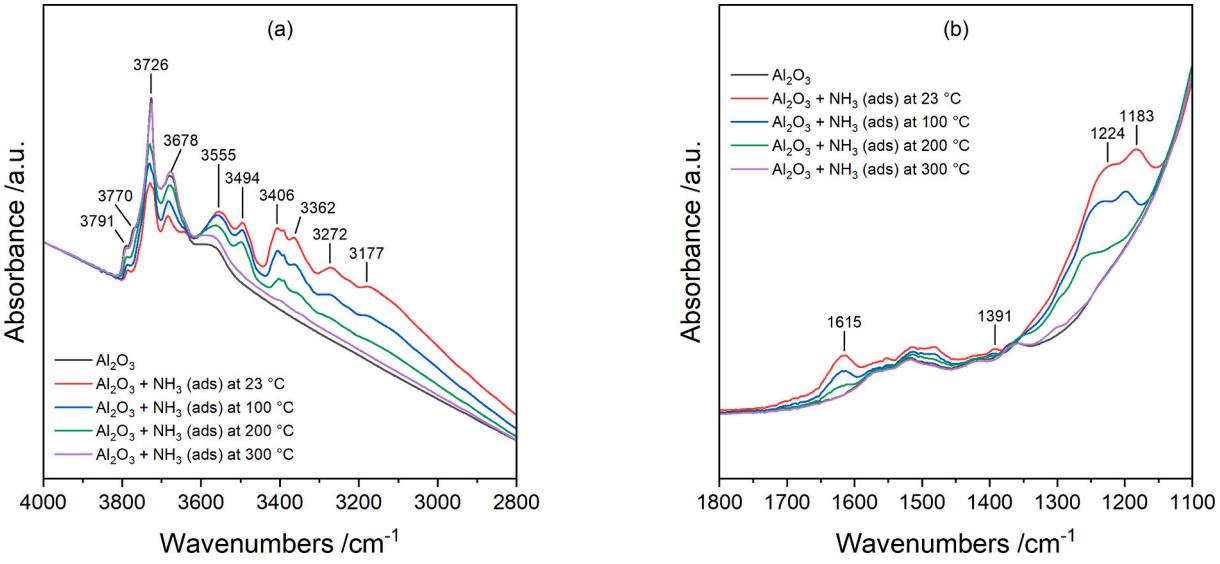

Fig. 4. FT-IR spectra of theta-alumina and subsequent ammonia adsorption in the stretching (a) and bending (b) domains at 23, 100, 200 and 300 °C.

3.2. *Pulse experiment*

18 injections of 1.15 µmol of isopropanol diluted in helium flow were carried out at 125 °C. Chromatograms do not show any other peaks than isopropanol, meaning that no reaction is taking place. Fig. 5 shows the evolution of calorimetric curves, and the adsorbed IPA followed by GC during successive pulses at 90 min intervals.

Each calorimetric curve shows a first very small endothermic peak visible just before each exothermic peak, which can be assigned to an artefact due to the switching of the 6-port valve. This event causes a brief drop in pressure in the pipe as a pressure difference occurs between the loop and the cell reactor line. This artefact, which is visible in every calorimetric curve, was not considered for the deconvolution.

During the first injection, a wide isopropanol peak of low intensity was detected by GC and only an exothermic peak was observable in the calorimetric curves, meaning that most isopropanol was strongly adsorbed on the catalyst surface. For the second pulse, the GC intensity of the IPA peak increased while the initial exothermic signal is followed by an endothermic peak in the corresponding calorimetric curves. With the following pulses, the exothermic peak continuously decreases while the endothermic signal increases (in absolute value). Besides, the amount of isopropanol adsorbed per pulse reaches a constant value of (17.7 ± 0.6) µmol · g^{-1}, which represents 24.7 % of the total injected amount. No visible changes and reproducibility of injections are reached after 9 pulses.

Injections 1 to 9 are linked to surface coverage of the catalyst until saturation of sites able to irreversibly and strongly adsorbed IPA. The non-selective adsorption of isopropanol on both strong and weak sites of the catalyst surface occurs for each injection. However, isopropanol that adsorbs weakly, desorbs back into the He carrier. Thus, the isopropanol which remains bonded is associated only with chemisorbed molecules. In the relatively short time of isopropanol exposure to the solid, the physisorbed molecules may not be able to migrate on the surface to occupy the most thermodynamically favorable sites, explaining the observed reversible adsorption before total surface coverage. This accounts for the adsorption is under kinetic control in the conditions of this study. Such phenomenon, which decreases in intensity with temperature, was previously observed in static calorimetry [48].

After reaching no changes between pulses answer, the adsorbed amount per dose is far from negligible. This value ((17.7 ± 0.6) µmol ·

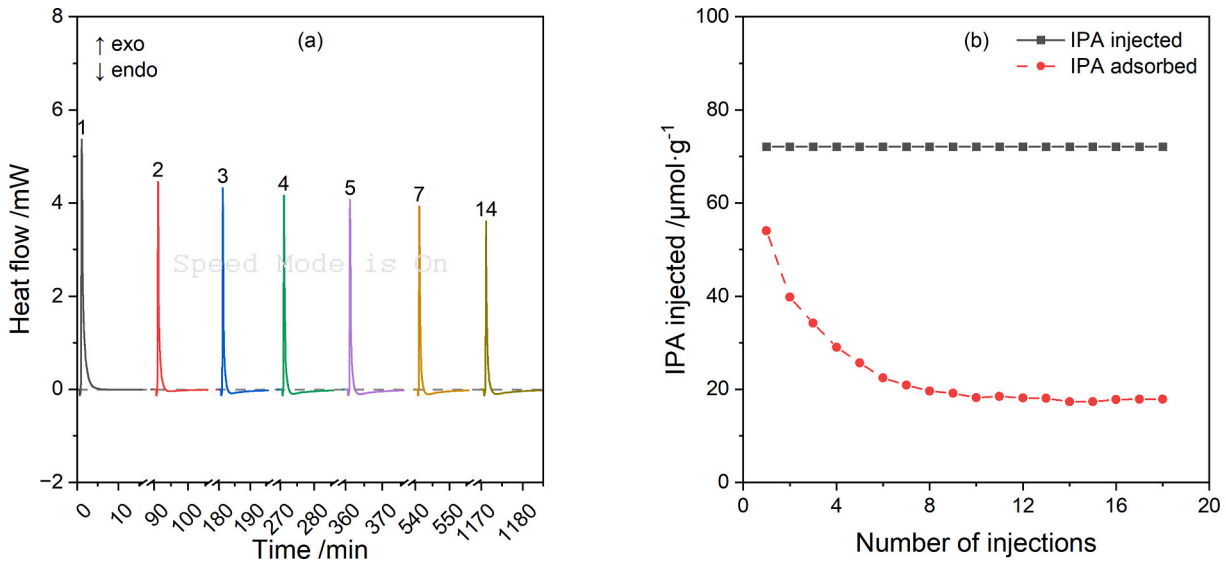

Fig. 5. Heat flow signals as a function of time and injection number (a) and injected (black) and adsorbed (red) quantities of IPA as a function of the injection number (b) after successive pulses of isopropanol every 90 min at 125 °C. For clarity, breaks in time are applied (a). (For interpretation of the references to colour in this figure legend, the reader is referred to the web version of this article.)

g^{-1}) is linked to a slow desorption of relatively weekly adsorbed isopropanol under the continuous flow of helium and represents the reversible adsorbed isopropanol. This effect is specific to flow adsorption methods as, after the reagent pulse has crossed the catalyst bed, the partial pressure of isopropanol in the gas is low and the relatively weakly adsorbed molecules that escape from the surface are carried towards the GC by the carrier gas [2]. The tail of the GC peak is also difficult to estimate as the flowing gas is flushing the catalyst during 90 min.

To differentiate adsorption and desorption of the reagent, heat flow signal deconvolution is performed as presented in Fig. 6. Compared to other models (chi-squared distribution (Fig. S2) and log-normal distribution (Fig. S3)), applying the 2 Fraser-Suzuki functions allows for the deconvoluted endothermic and exothermic peaks to start at the same time. This is in line with the weak probe character of isopropanol (dissociation constants of IPA in aqueous solution at 25 °C are 17.1 (acidic) and − 3.1 (basic) versus pKa of 1.89 and 9.24 for SO_2 and NH_3, respectively). Thus, the used deconvolution method underlines the simultaneity of both the adsorption and the desorption phenomena effects. The coefficient of determination is adequate as it reaches a value of 0.994.

For the 16.0 mg of catalysts loaded, the exothermic peak is well defined with a maximum intensity of 3.58 mW and lasts approximately 3.3 min. On the other hand, the endothermic peak associated with desorption has a very low intensity of −0.10 mW but is spreading considerably above 15 min. These first observations already indicate the kinetic difference between the fast exothermic adsorption process and the slow endothermic desorption induced by the constant flushing of the catalyst surface.

The slow desorption of isopropanol under the helium flow is confirmed by integration of the heat flow signal as shown in Fig. 7 (a). The integrated energies corresponding to the exothermic and endothermic signals, as well as the sum of both calorimetric curves, follow the same trend, with a slow decrease from +165 to +93 mJ, from 0 to −88 mJ and from +165 to +38 mJ respectively up to the 9th injection.

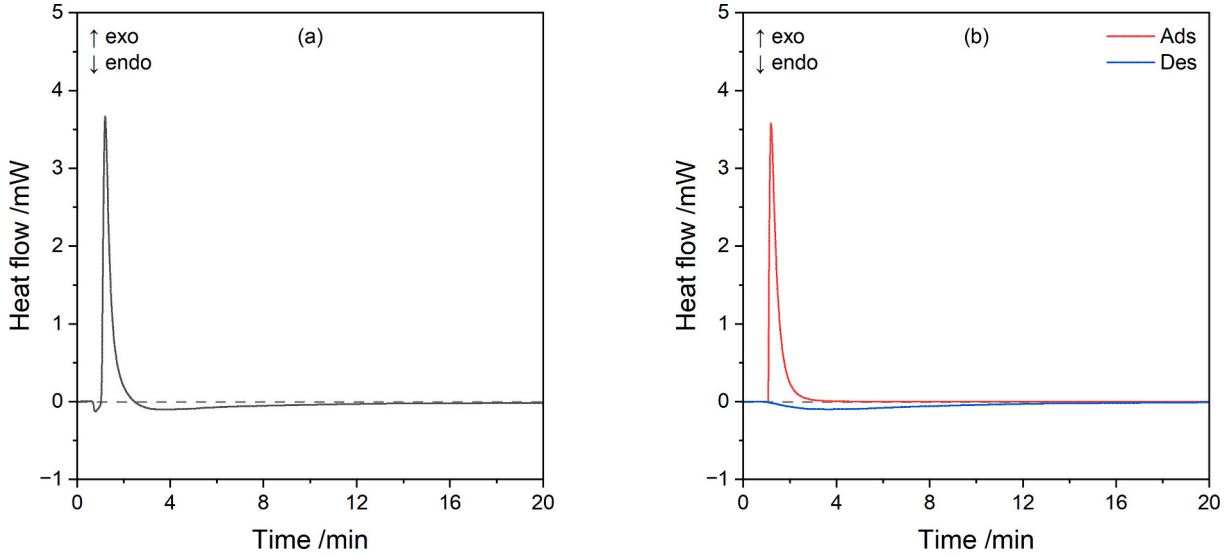

Fig. 6. Typical recorded (a) and deconvoluted (based on Fraser-Suzuki functions) (b) heat flow signal as a function of time when no reaction occurs and the reproducibility of pulses is reached (last pulse, number 18, at 125 °C).

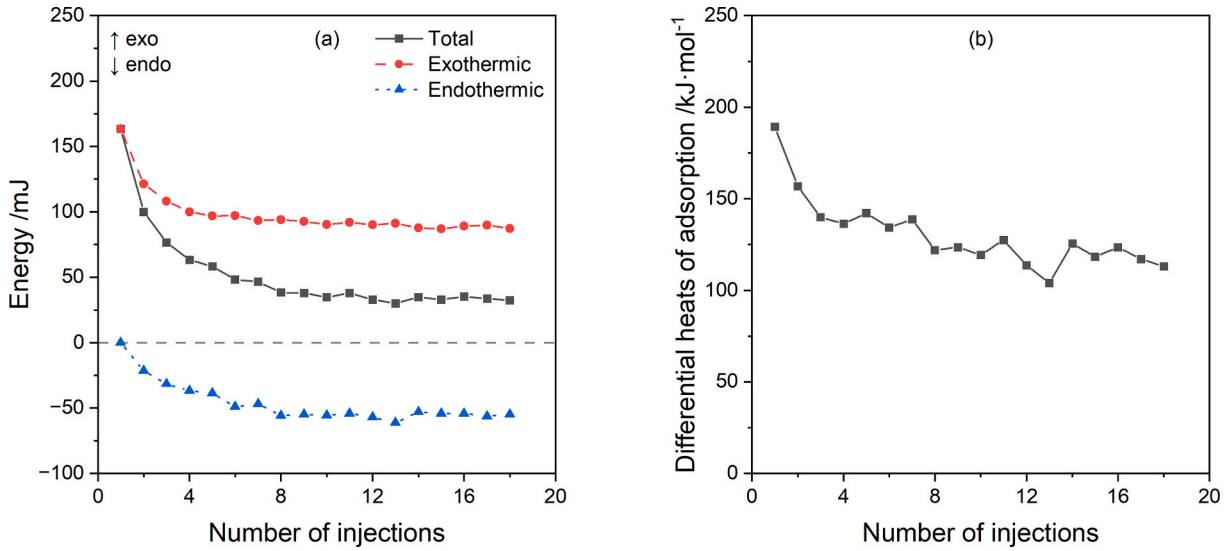

Fig. 7. Integrated energy (a) and differential heats (b) as a function of the injection number at 125 °C for 16.0 mg of sample.

If no adsorption of isopropanol occurs on the surface, the global energy should be equal to 0 as the endothermic desorption should compensate for the exothermic adsorption. However, above 10 injections, the energy remains positive after reaching reproducibility of pulses.

This observation is in line with chromatographic results as it may be a consequence of a slow and undetectable desorption occurring over time. The global differential heat of adsorption decreases (in absolute value) from −189 to −123 kJ · mol^{-1} from the first to the 9th injection, then reaches a plateau with an average value of −118 ± 5 kJ · mol^{-1} as shown in Fig. 7 (b).

The catalyst surface occupied by the adsorbed isopropanol S_{IPA}^{occ} can be calculated as follows (Eq. 11):

$$S_{IPA}^{occ} = \frac{\pi \cdot \phi_{IPA}{}^2 \cdot n_{ads}^{IPA} \cdot N_A}{4} \quad (11)$$

with ϕ_{IPA} the kinetic diameter of isopropanol (0.47 nm [57]), n_{ads}^{IPA} the quantity of adsorbed IPA and N_A the Avogadro constant. After 9 injections, the total adsorbed amount is 265 µmol · g^{-1}, resulting in a total surface occupied of 28 m^2 · g^{-1}, i.e. 24 % of the total available surface.

The differential heat value for the first pulse (− 189 kJ · mol^{-1}) is within the range of typical dissociative chemisorption and could correspond to bidentate alkoxide formations as presented in Fig. 8 (a) [58,59].

The average value at the plateau (− 118 ± 5) kJ · mol^{-1} is very high if only physical adsorption is expected. In static studies, the heats of adsorption usually decrease (in absolute value) until they approach the latent heat of isopropanol liquefaction (− 39 kJ · mol^{-1} at 121 °C) [60].

Coordinative adsorption, or ligand adsorption, could explain this margin as their typical heat is between – 120 and – 70 kJ · mol^{-1} [58]. Coordinative adsorption is not reversible at room temperature, but Fubini et al. [58] noticed reversibility at 100 °C for water on alumina. Larmier et al. [64] and Feng et al. [65], through density function theory (DTF), calculated an adsorption heat between – 88 and – 121 kJ · mol^{-1} on Al atoms depending on coordination modes. According to Larmier et al. [64], isopropanol adsorbs preferentially in the form of a coordinated alcohol on partially hydrated surface. Then, a dissociation of the O − H bond can go through a reversible and activated process of only 3

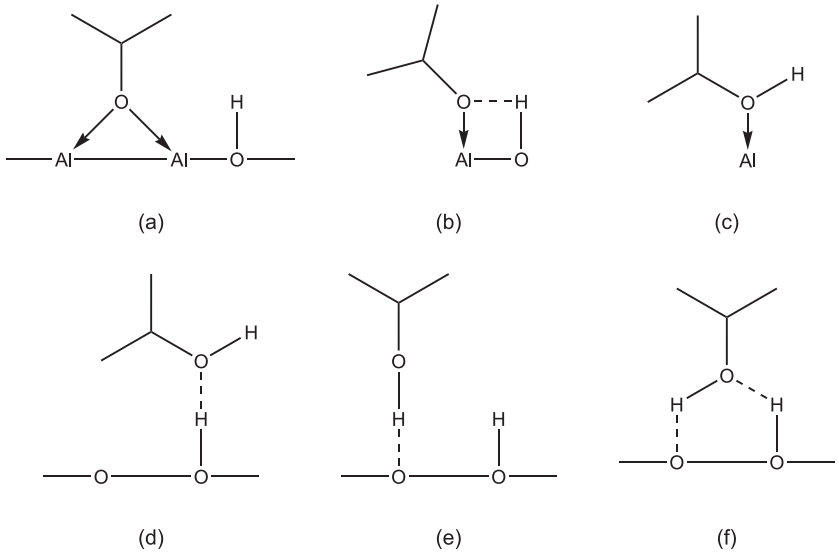

Fig. 8. Types of adsorbed isopropanol on alumina sites: dissociated bidental alkoxide (a) dissociated linear alkoxide (b), non-dissociated coordinated alcohol (c), hydrogen bond on oxygen (d) hydrogen bond on a hydroxyl group (e) and double hydrogen bond on both a hydroxyl group and oxygen (f). [52,61–63].

kJ · mol^{-1} as show in Fig. 8 (b). The observed reversibility, however, favours the idea of coordinated alcohols adsorption as shown in Fig. 8 (c), which is the step prior to dissociation.

A very strong hydrogen bond formation with the oxygen and hydroxyl groups of the catalyst surface could also be responsible for this relatively high value, while explaining the reversibility under helium flow. Similar effects were observed by Gale et al. [66] for isopropanol adsorption on nickel oxide and Beebe et al. [67] for the adsorption of methanol and water on hydroxyapatite. The OH groups from isopropanol and the basic sites of the amphoteric alumina are expected to strongly favour these types of bonds. Knözinger [61] reviewed the different studies done on molecular adsorption of alcohols on alumina and proposed the 3 different hydrogen adsorption types as displayed in Fig. 8 (d), (e) and (f). Heat values at higher coverage are too high to be explained by simple hydrogen bonds on surface oxygens (d) and hydroxyls (e) adsorption, usually −30 to −70 kJ · mol^{-1}. Adsorption on both surface sites (f), on the other end, will be more stable than single-bond types. They may explain the relatively high heat of adsorption for a hydrogen bond and may compete with coordinative adsorption from Fig. 8 (c).

Fig. 9 displays the calorimetric curves obtained at increasing DSC temperature and respective TCD chromatograms. Table 1 shows the conversion based on isopropanol consumed from FID results. Carbon balances were 97.6 %, 96.9 % and 98.8 % at 200 °C, 225 °C and 250 °C respectively.

The increase in temperature leads to an increase in the endothermic peak area and a reduction in its width, unlike the exothermic peak, which shape remains almost identical but narrower/sharper. This is the expected behavior for the endothermic peak, as the triggered reaction of dehydration to propylene is endothermic. The endothermic peak enhancement is explained by the fact that isopropanol dehydration on the surface (meaning dissociation into water and propylene) and desorption of adsorbed products from the surface are both endothermic. However, only one endothermic peak is observed as the overlapping of multiple endothermic peaks can be expected: the reaction, the desorption of water, and the desorption of propylene (only the formation of diisopropyl ether would be exothermic, but it is not detected by GC or below detection limit). Although, depending on the reaction mechanism – Langmuir or Eley Rideal – propylene could be considered as adsorbed or not. The absence of multiple endothermic peaks could also be explained by an Eldey-Rideal type mechanism, so that propylene and/or water are not adsorbed on the catalyst surface but directly released in the gas phase.

Table 1
Isopropanol conversion rate at studied temperatures.

Temperature/°C	Conversion/% ± 3
175	85
200	87
225	92
250	95

The time difference between the exothermic and endothermic peak maximums could be an estimation of the mean residence time on the surface. This time can be roughly calculated as 2.55, 1.97 and 0.87 min at 200, 225 and 250 °C respectively.

On the other hand, the TCD signal clearly shows the presence of water starting from 175 °C, indicating that a dehydration reaction is taking place. A propylene peak is also visible in TCD signals, but in the form of an extremely wide peak of low intensity that spread over the entire 90-min analysis time, making its quantification impossible. Finally, a peak of DIPE under quantification limit is observed. It is not possible to check if carbon balance is reached at 175 °C: reaction products, meaning propylene and diisopropyl ether (thermodynamically favoured at low temperature) can remain adsorbed on catalyst surface.

The propylene peak, at a retention time of 3.00 min, shows an increase in peak maximum intensity and a considerable reduction in peak width when temperature is increased. The same trend is followed by the endothermic peak in the calorimetric curve. Water peak shape, at a retention time of 2.35 min, does not present a significant change in shape at 175, 200, 225 and 250 °C. As GC parameters are not modified when DSC temperature changes, the observations regarding the propylene peaks would be linked to the temperature changes of the reactor. Propylene seems to be dependent on temperature compared to water formation/desorption and might indicate that propylene formation or desorption is the limiting step of the dehydration reaction on θ-alumina catalyst.

The rapid release of water followed by a slower production of alkenes on an alumina catalyst has also been observed by Moravek and Kraus [68] through transient response techniques, such as pulse flow and stopped feed, with ethanol. The authors concluded that, on alumina catalyst, surface ethoxide is the reaction intermediate for dehydration of ethanol to ethylene and diethyl ether. Alkoxide is formed by the

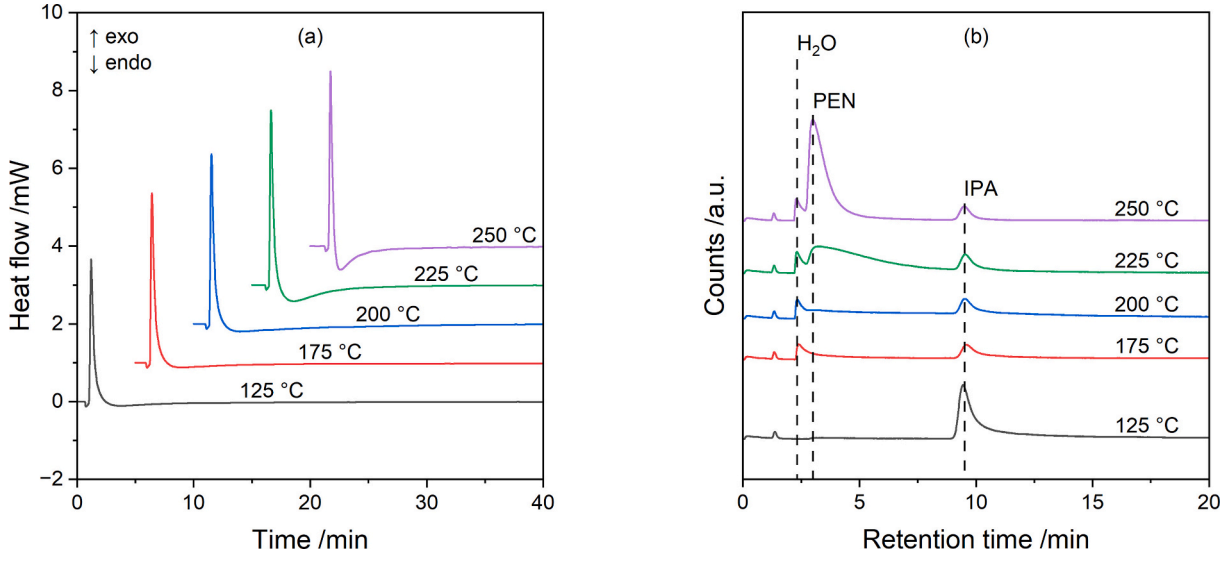

Fig. 9. Heat flow (a) and TCD (b) signals for injection number 9 at reaction temperatures and at 125 °C (black) for comparison, as a function of time and temperature. For clarity, offsets are applied on heat flow, time (a) and counts (b).

substitution of a surface hydroxyl group by the alcohol on the catalyst surface. Water is liberated and a relatively slow decomposition of alkoxides to alkenes takes place.

This rapid desorption of water could also be due to the competitive adsorption of IPA during the first moments of injection as the IPA displaces the water out of adsorption sites. A separate experiment was performed on water adsorption/desorption on a fresh catalyst and with an empty reactor, in the absence of isopropanol.

Fig. 10 compares the TCD signals obtained at 250 °C with a pulse of water in an empty reactor (in the calorimeter), pulse of water on alumina and pulse of isopropanol on alumina (nIPA/inj = 1.15 µmol and nH_2O/inj = 0.797 µmol). Water retention time is increased from 2.17 min with an empty reactor to 3.15 min with a loaded alumina catalyst. In the absence of catalyst, the water peak maximum intensity is 22,678 counts and returns to baseline in 4 min. The presence of a catalyst causes a flow resistance and the peak maximum intensity to drop to 891 counts and takes much longer time to return to baseline, estimated at 18 min. The increase in retention time and peak broadening may indicate an increase in water residence time in the catalyst combined with a slow desorption of water from its surface during water adsorption/desorption, respectively.

The water peak observed when the reaction occurs shows a retention time of 2.35 min. Because of the overlapping between water and propylene peak, it is not possible to determine the exact width of the peak, but a return to the baseline in 6 or 8 min could be estimated. Although the load dump, intensity and peak width indicate some retention and desorption of the water produced by the reaction, its interaction with the catalyst surface seems to be less significant than water directly adsorbed/desorbed.

This shows that in the reaction conditions, water molecules produced are less strongly adsorbed than isopropanol on the catalyst surface. Isopropanol from the gas-phase will displace adsorbed water avoiding the formation of a network of hydrogen bonding and thus the strong adsorption of water as can be observed on the clean alumina surface. Standard heats of vaporization of water and isopropanol are 43.98 and 45.39 kJ · mol^{-1} respectively. The dipole moments are 1.83 D and 1.69 D for water and isopropanol respectively. These close values support the hypothesis of a competitivity between isopropanol and water adsorption on an amphoteric solid.

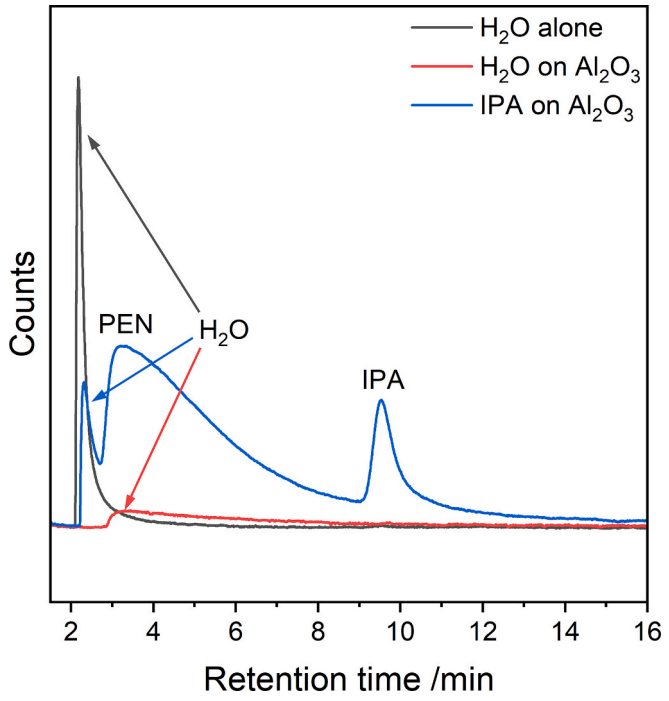

Fig. 10. TCD signals obtained at 250 °C when (i) a pulse of water was sent through an empty reactor (placed inside the calorimeter), (ii) a pulse of water was sent through the reactor containing alumina and (iii) a pulse of isopropanol was sent through the reactor containing alumina.

Fig. 11 shows the calorimetric curves and GC results obtained after successive injections of isopropanol at 250 °C.

Compared to previous results at 125 °C, reproducibility of pulses is reached after 3 injections and only a small decrease of exothermic signal and increase of endothermic peaks are observed. Selectivity for propylene is considered total as acetone and diisopropyl ether are detected only at trace levels and no other peaks were observed by GC.

The TCD chromatogram shows a pronounced increase of the water peak compared to propylene as injections occur (Fig. S4). This observation supports the idea that isopropanol displaces the adsorbed water produced during the previous injections. Isopropanol adsorption releases heat which can induce some water desorption. A correlation has been noticed between the exothermic contribution and water peak intensity in the chromatogram favoring this hypothesis. Considering the heat of condensation as an approximation for the heat of adsorption, the proximity of the values (43.98 and 45.39 kJ·mol^{-1} for water and isopropanol respectively) may explain that the adsorption of one is sufficient to meet the energy requirements for the desorption of the other.

The deconvolution of calorimetric curves was performed to differentiate the exothermic adsorption and endothermic reaction/desorption. Fig. 12 displays an example of deconvolution on the 6th injection calorimetric curve at 250 °C.

As observed above, the Fraser-Suzuki 2-function model allows the exothermic and endothermic peaks to be initiated at the same time with a coefficient of determination of 0.994.

The exothermic signal is close to that observed at 125 °C, while the endothermic peak is significantly more prominent as the minimum is at −0.76 mW (instead of −0.10 mW) and spread on 10 min only (instead of 15 min).

The differential exothermic and endothermic heats obtained after integration at given temperatures are presented in Table 2.

As the conversion level increases with temperature (Table 1), the exothermic and endothermic heats shown in Table 2 are sightly decreasing (in absolute value). Average values considering the three studied temperatures are – 100 kJ · mol^{-1} IPA reacted and + 121 kJ · mol^{-1} PEN produced for respectively the exothermic and the endothermic effects. Considering that the reaction enthalpy is constant in the studied temperature range (the enthalpy change ranges from 52.91 to 52.71 kJ mol^{-1} as the temperature increases from 200 to 250 °C, respectively, as calculated from Kirchhoff's Law), only the desorption of propylene and water is modified with temperature.

The average exothermic heat of adsorption is close to that obtained at 125 °C ((− 118 ± 5) kJ · mol^{-1}) when no reaction occurred. The slight decrease (in absolute value) between – 118 and – 92 kJ · mol^{-1} can be explained by the increase in temperature, which displaces the equilibrium, and by the increase in water coverage of the catalyst's strongest active sites.

In endothermic peaks, reaction and desorption of supposed weekly adsorbed propylene and water contribute to the heat flow. Therefore, the endothermic value (ΔH_{endo}) should be equal to the sum of the reaction enthalpy and desorption heats of propylene and steam (Eq. 12).

Assuming that the desorption enthalpy of the products is close to the corresponding vaporization enthalpy,

$$\Delta H_{endo} = \Delta_r H^{250°C}_{1\ atm} + \Delta_{vap} H^{PEN} + \Delta_{vap} H^{H_2O} \quad (12)$$

A theoretical value can be calculated (Eq. 13):

$$\Delta H_{endo} = 53 + 21 + 44 = 118\,kJ{\cdot}mol^{-1} \quad (13)$$

Reaction enthalpy was calculated using the standard enthalpies of formation and corrected at the reaction temperature using heat capacity of products and reactant [69].

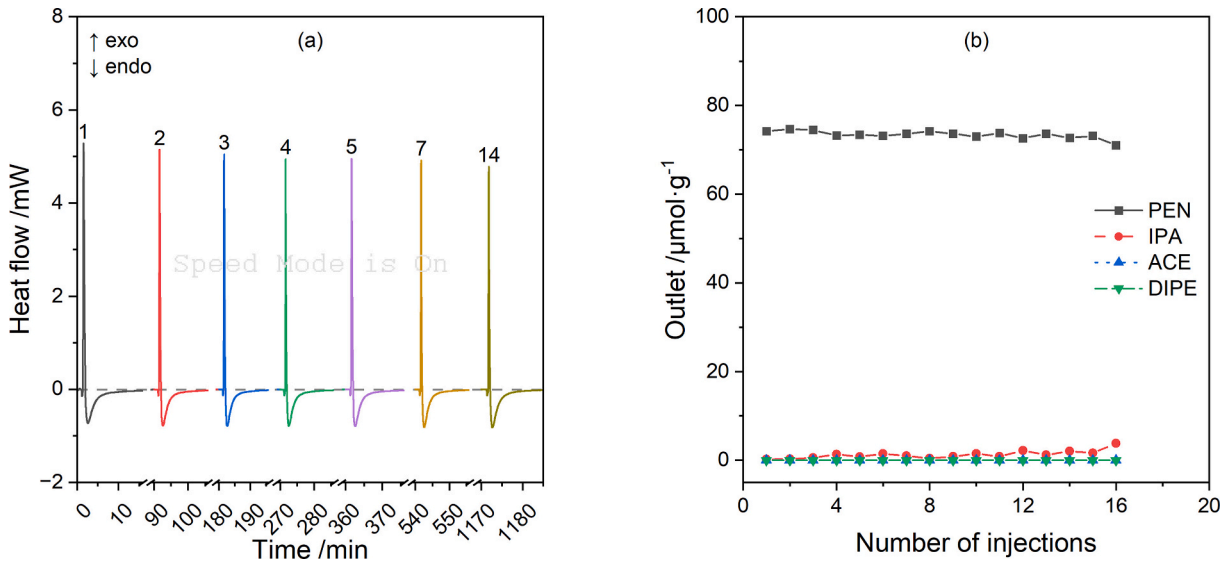

Fig. 11. Heat flow signals as a function of time and injection number (a) and reactor outlet GC quantities as a function of the injection number (b) after successive pulses of isopropanol every 90 min at 250 °C. For clarity breaks in time are applied (a).

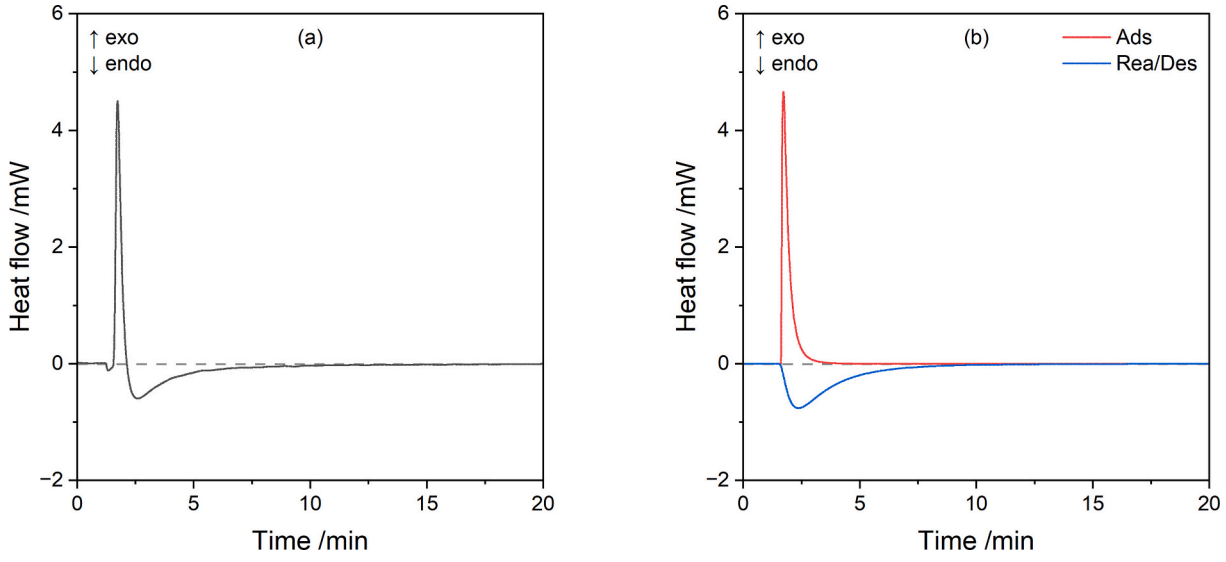

Fig. 12. Typical recorded (a) and deconvoluted (b) heat flow signal as a function of time when reaction occurs and when reproducibility of pulses is reached (injection number 6 at 250 °C).

Table 2
Calorimetric curves results.

Temperature /°C	Exothermic heat /kJ·mol_{IPA}^{-1} ± 5	Endothermic heat /kJ·mol_{PEN}^{-1} ± 5
200	- 105	+ 122
225	- 101	+ 129
250	- 92	+ 112

Value of propylene desorption heat was taken from Casquero Ruiz et al. [70]. who calculated the isosteric heat of adsorption of multiple hydrocarbons on a γ-alumina sample using a volumetric apparatus. For propylene, the value obtained at maximum coverage, meaning mainly physisorption, is (heat of adsorption) − 21 kJ · mol^{-1}. This value is close to the latent heat of liquefaction of −19 kJ · mol^{-1} at 67 °C [71].

The heat of adsorption of steam on oxides was studied by numerous authors, including Rossi et al. [72] and Fubini et al. [58]. They agree that, at high coverage, the heat of adsorption always drops to −44 kJ · mol^{-1} for oxides corresponding also to the latent heat of liquefaction of water at 25 °C.

The calculated value of +118 ± 4 kJ · mol^{-1} is rather close to the measured value ((+ 121 ± 4) kJ · mol^{-1}), which supports the stated thermal contributions of the endothermic peak and the coordinative adsorption mode. Indeed, if the adsorption mode was strongly dissociative, it would have resulted in a significant difference in the enthalpy of reaction as the standard reaction enthalpy considers bond dissociations.

3.3. Advanced isoconversional kinetic analysis

The reaction rates and extents of conversion for the exothermic peaks are presented in Fig. 13. Friedman's and Vyazovkin's methods were then applied to these data and the resulting E_α values are presented in Fig. 14. The two methods give similar results, thus only the results of the NLN

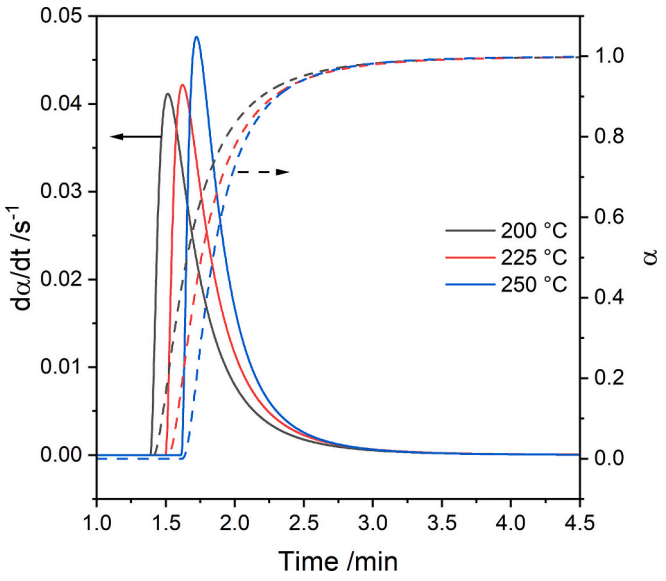

Fig. 13. Reaction rate ($d\alpha/dt$) (left) and extent of conversion (α) (right) of the exothermic peak as a function of time (t) for three temperatures (200, 225 and 250 °C).

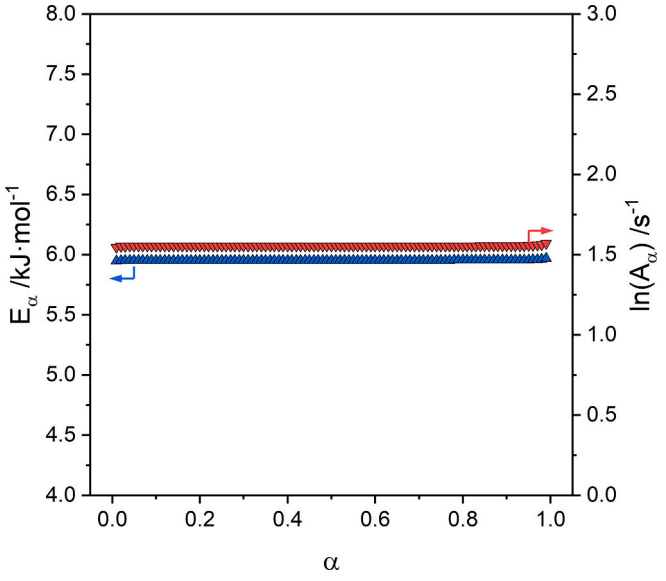

Fig. 14. Variation of E_α (left, solid symbol) and of $\ln(A_\alpha)$ (right, open symbol) vs. extent of conversion (α) for the adsorption.

method are presented in this figure for clarity. Fig. S5 gives the plots obtained for the three models used in the compensation effect (CE). The linearization of the models used for the CE is presented in Fig. S6. A good linearization of the data is obtained for the models F1, R2 and R3 [28,38,42]. These models respectively correspond to first order reaction (Mampel), contracting cylinder and contracting sphere. The principle of the CE is to establish a linear relationship between $\ln(A)$ and E_a, to compute $\ln(A_\alpha)$ in a model-free way using the values of E_α obtained using an advanced isoconversional method.

Interestingly, the E_α and $\ln(A_\alpha)$ dependencies do not show any variations on the whole extent of conversion interval. This case is extremely rare and indicates that a single mechanism dominates in this temperature domain. The very low E_α values are more likely related to a physical transformation than to a chemical reaction [38]. Activation energy of dissociative chemisorption generally range between 50 and 100 kJ · mol^{-1} [58]. It is concluded that the rate-limiting step is more related to diffusion or surface penetration processes, which would result in low E_α values and agrees with the hypothesis of a single-step process. Thus, for temperatures between 200 and 250 °C, diffusion could be the rate-limiting step of the overall adsorption process as measured by calorimetry. The low activation energy supports the non-dissociative adsorption process. The 6 kJ · mol^{-1} determined in Fig. 14 are in good agreement with Larmier's results and can support the hypothesis that isopropanol first adsorbed non-dissociatively before the formation of a deprotonated alkoxide [64].

Fig. 15 gives the variations of the mathematical function $f(\alpha)_\alpha$ that represents the reaction model with the extent of conversion. Note that each α value was computed in a model-way according to the method described in [42,43]. These variations are very close to a Sestak-Berggren model with $m = 0.5$ and $n = 1.5$. Indeed, in the truncated Sestak-Berggren model $f(\alpha)$ is expressed as [42]:

$$f(\alpha) = \alpha^m (1-\alpha)^n \tag{14}$$

This model is usually used to describe reactions in the solid state [73]. The reaction rates and extents of conversion of the endothermic peaks are presented in Fig. 16. The resulting E_α and $\ln(A_\alpha)$ dependencies are presented in Fig. 17. Fig. S7 gives the plots obtained for the three models used in the compensation effect (CE). The linearization of the models used for the CE is presented in Fig. S8. The best fits are obtained for models F2, SB, F1, R2 and R3 [28,38,42]. These models respectively correspond to second order reaction, truncated Sestak-Berggren model ($m = 0.5$, $n = 1.5$), first order reaction, contracting cylinder and contracting sphere.

At the initial stage of the reaction, a value of E_α of around 60 kJ · mol^{-1} is found. This value is typical of chemical reactions [38] and can be attributed to the catalytic dehydration of isopropanol to propylene. For $\alpha > 0.50$, a decrease to very low E_α values is observed.

This decrease is characteristic of a control of the overall reaction by the diffusion of small molecules [32,41]. Thus, it is concluded that the overall reaction involves several rate-limiting steps. The initial steps of the reaction are dominated by chemical reactions with catalysis, while for $\alpha > 0.50$ the diffusion becomes limiting, and the overall reaction rate

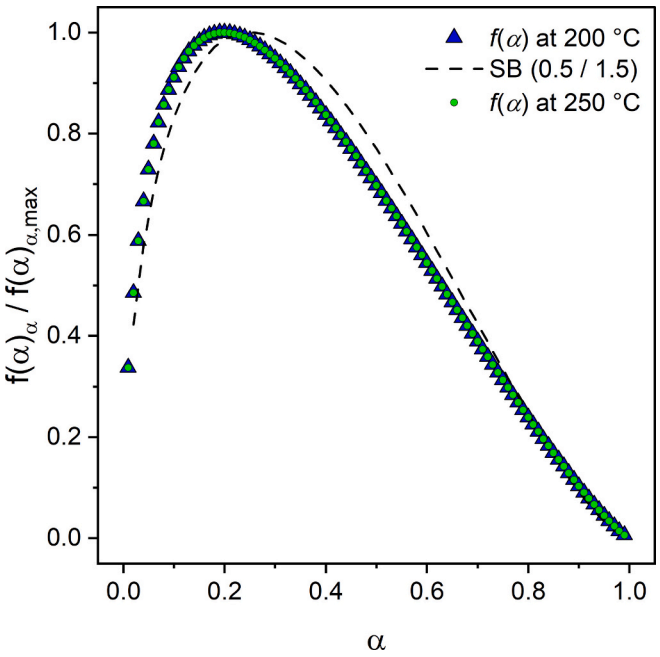

Fig. 15. Normalized variations of the mathematical function $f(\alpha)_\alpha$ that represents the reaction model with extent of conversion (α) at 200 °C (triangle) and 250 °C (circle). Dash: theoretical values for SB's model with $m = 0.5$ and $n = 1.5$.

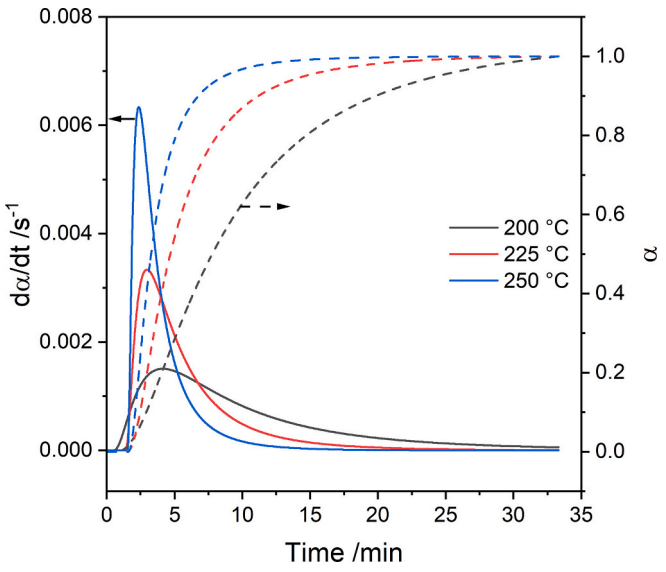

Fig. 16. Reaction rate ($d\alpha/dt$) (solid, left) and extent of conversion (α) (dash, right) as a function of time (t) at three temperatures (200 °C, 225 °C and 250 °C) for the endothermic peaks.

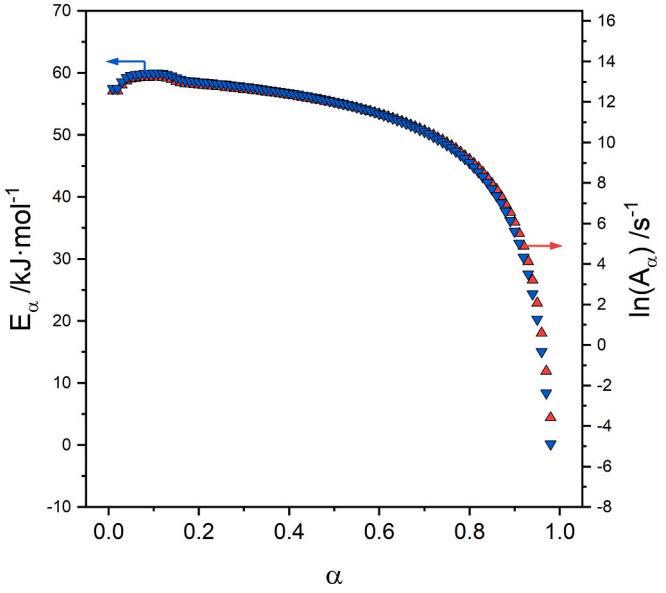

Fig. 17. Variation of E_α (left, solid symbol) and of $\ln(A_\alpha)$ (right, open symbol) vs. extent of conversion (α).

is an interplay between chemical reactions and diffusion rates. Differences in the residence time of propylene and water on the catalyst surface were observed, highlighted by the times of the desorption peaks. The last reacting isopropanol molecules are in an environment rich in adsorbed water molecules, while propylene is already desorbed. This environment should play a role in the adsorption/desorption equilibrium.

The calculated activation energy for $\alpha < 0.50$ (60 kJ · mol^{-1}) is rather low compared to values obtained by conventional Arrhenius plot in the literature (125 kJ · mol^{-1}) [8,64].

To rule out the hypothesis that internal transfer limitation takes place, which would result in an apparent activation energy equal to half the reaction activation energy [74], another experiment with lower particle diameters (180–300 µm) was performed and compared to previous results (300–425 µm). Similar conversion level and no significant change in the calorimetric signals refute internal transfer limitation hypothesis as shown in Table S1 and Fig. S9. Thus, to explain this difference, the differences in experimental conditions must be considered. Indeed, the steady-state experimental conditions of literature are far from those of the pulse, i.e. conversion rate, temperature and partial pressure of the reactant, which may lead to a different limiting step or to a different mechanism.

The variations of the mathematical function $f(\alpha)_\alpha/f(\alpha)_{\alpha=0.29}$ that represents the reaction mechanism is presented in Fig. 18. These variations are complex and do not correspond to any known model. This confirms the hypothesis of a multi-step process. However, the initial part of the reaction ($0.10 < \alpha < 0.50$) is perfectly described by a SB model with $m = 0.50$ and $n = 1.00$ (Fig. 18). This corroborates the hypothesis of catalytic reactions for $\alpha < 0.50$.

Following the conclusions drawn from the advanced isoconversional kinetic analysis, the overall reaction rate is an interplay between catalytic reactions and diffusion of small molecules.

To check this hypothesis and to go further in the modelling and the understanding of the mechanisms of the reactions, a model including a catalytic step and a diffusion step was used to describe the reaction rates as measured by calorimetry. The mathematical equations of this model adapted from the original Vyazovkin-Sbirrazzuoli's model (MSM) are described below ((Eq. 15) and (Eq. 16)) [41,44]:

$$k_c(T) = A_1 \exp\left(-\frac{E_1}{RT}\right) \tag{15}$$

where k_c is the rate constant of the chemical step, E_1 and A_1 are respectively the activation energy and pre-exponential factor of this step.

$$k_D(T,\alpha) = D_0 \exp\left(-\frac{E_D}{RT} + K\alpha\right) \tag{16}$$

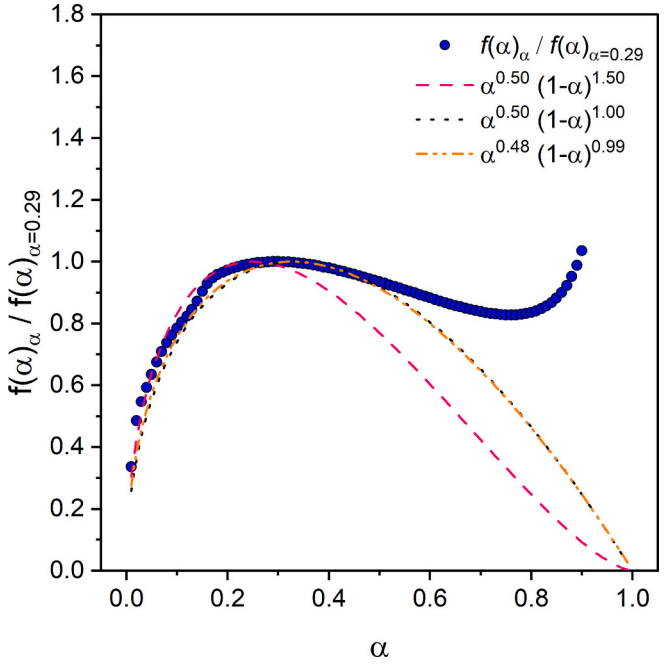

Fig. 18. Normalized variations of the mathematical function $f(\alpha)_\alpha/f(\alpha)_{\alpha=0.29}$ that represents the reaction model with extent of conversion (α) at 200 °C (circle). Theoretical values for SB's model with $m = 0.50$ and $n = 1.50$ (red, dash), with $m = 0.50$ and $n = 1.00$ (black, dot), with $m = 0.48$ and $n = 0.99$ (orange, dash dot dot). Values of $f(\alpha)_\alpha$ for $\alpha > 0.90$ are not given as the CE was calculated for $0.10 < \alpha < 0.90$ (best linearization). (For interpretation of the references to colour in this figure legend, the reader is referred to the web version of this article.)

where k_D is the rate constant of the diffusion step, E_D and D_0 are respectively the activation energy and pre-exponential factor of this step. Then, the overall reaction rate is obtained by (Eq. 17):

$$k_{ef}^{-1} = k_C^{-1} + k_D^{-1} \quad (17)$$

and the overall reaction rate given by (Eq. 18):

$$\frac{d\alpha}{dt} = k_{ef}\, \alpha^m (1-\alpha)^n \quad (18)$$

where m is the catalytic exponent and n a reaction order. This model refers to Modified Vyazovkin-Sbirrazzuoli's model (MVSM).

All the parameters of this model were obtained from the fitting of the experimental reaction rate curves (Fig. 19). The initial values of E_1, A_1, E_D and D_0 were selected using the extremal values given by the advanced isoconversional kinetic analysis [40,41]. This greatly facilitates the choice of the initial parameters for optimization and limits the problem of local minima [75]. The variance was estimated to characterize the validity of the rate fits as (Eq. 19) [75].

$$S^2 = \frac{\sum_{i=1}^{N}\left[\left(\frac{d\alpha}{dt}\right)_{exp,i} - \left(\frac{d\alpha}{dt}\right)_{calc,i}\right]^2}{N-p} \quad (19)$$

where $(d\alpha/dt)_{exp,i}$ and $(d\alpha/dt)_{calc,i}$ respectively are the experimental and model values of the reaction rate, N is the number of experimentally measured values and p is the number of adjustable parameters of the model. The parameters are given in Table 3.

The values of E_1, E_D, m and n are consistent with a model that combines catalysis and diffusion. Indeed, we found E_1 higher than E_D, and a value of E_1 (74 kJ · mol^{-1}) in the order of magnitude for a chemical reaction, close to E_α when α is close to 0, i.e. 60 kJ · mol^{-1}. The values of m and n are typical of catalytic reactions. The negative value of K is also consistent with the diffusion of small molecules. The values obtained after nonlinear fitting are not only fitting parameters, but meaningful kinetic parameters giving insight in the reaction mechanism. Note that the values of m and n are very close to the theoretical values $m = 0.50$ and $n = 1.00$ of the SB model presented in Fig. 18, which also validates the consistency of the two very different computational approaches used. As seen in Fig. 19, the model perfectly describes the experimental data.

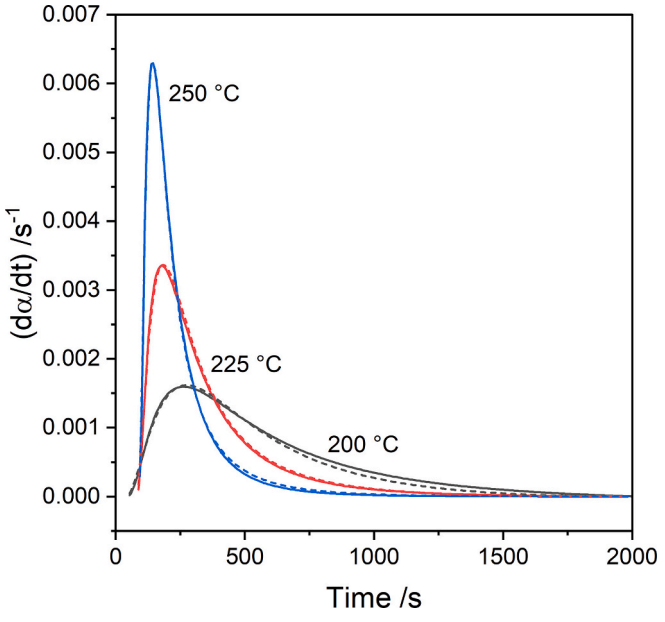

Fig. 19. Fits obtained after optimization of (Eq. 18). Experimental data: solid lines; fits: dash lines. Modified Vyazovkin-Sbirrazzuoli's model (MSM).

A more complex model has been tested in this study: the Vyazovkin-Sbirrazzuoli's model (VSM) [32,44]. This model differs from the previous model for the expressions of k_c and $d\alpha/dt$:

$$k_c(T,\alpha) = A_1 \exp\left(-\frac{E_1}{RT}\right) + A_2 \exp\left(-\frac{E_2}{RT}\right)\alpha^m \quad (20)$$

E_1, E_2 and A_1, A_2 are respectively the activation energies and pre-exponential factors of this step,

$$\frac{d\alpha}{dt} = k_{ef}\,(1-\alpha)^n \quad (21)$$

The values of the parameters are given in Table 4. This model is more complex and requires optimization of 9 parameters instead of 7. However, it provides little improvement of the quality of the fits, as reflected by the slightly lowest value of S^2. Obtaining the convergence of 9 parameters is not an easy task, especially if meaningful parameters are desired and not only fitting parameters. To achieve this goal, the parameters of Table 3 were taken as initial values before optimization.

The values of E_1, E_2, E_D, m and n are still consistent with a model that combines catalysis and diffusion. The value of E_1, attributed to the non-catalyzed part of the reaction is higher than E_2, which corresponds to the catalyzed part of the reaction. The accuracy of the fit is presented in Fig. S10.

A mechanism as described by the Modified Vyazovkin-Sbirrazzuoli's model can correspond to a E2 mechanism, and the 74 kJ.mol^{-1} value corresponds to the abstraction of the H_β and cleavage of the $C_\alpha - O$ bond as exposed in Fig. 20 (d).

On the other end, a two-step mechanism as described by the Vyazovkin-Sbirrazzuoli's model gives a first activation energy of 143 kJ.mol^{-1}, which is closer to the values obtained in literature (i.e. 125 kJ · mol^{-1}) and could correspond to the limiting step during steady state experiments.

Note that the difference is explained by the hypothesis of a single-step process in the conventional method.

An $E1_{cb}$ mechanism is most likely as presented in Fig. 21. The first activated E1 step is the abstraction of the H_β (d), leading to the formation of a surface carbanion (e). The second activated step E2 of 63 kJ · mol^{-1} correspond to the C − O cleavage (f) leading to the formation of propylene (g).

The $E1_{cb}$ mechanism requires stronger basic sites compared to E2 mechanism to allow for H_β abstraction [35]. The wide distribution of acidity and basicity of the θ-Al_2O_3 expects to favour $E1_{cb}$ mechanism. Considering the variety of the acid-base surface sites of the used alumina, it cannot be rejected that both mechanisms take place at the same time. In both mechanisms, alcohol deprotonation and water recombination, respectively (b) and (f) in Fig. 20 and (b) and (h) in Fig. 21 are considered poorly activated processes.

4. Conclusion

The coupling of a pulse catalytic test set inside a calorimeter and linked to a gas chromatograph was used to study the catalytic dehydration of isopropanol to propylene over an alumina catalyst. Tests were carried out at different temperatures: 125 °C, where only adsorption and desorption of isopropanol were observed, and at 200 °C and above, where selective dehydration to propylene takes place. Analyzing the obtained chromatograms and calorimetric curves allowed to gain lights on the adsorption, desorption, and reaction heats and processes. Further advanced computational studies on the heat signals allowed to determine meaningful kinetic parameters.

Under helium flow, isopropanol is adsorbed in a coordinated, non-dissociative manner in the range of 125 °C to 250 °C. The low activation energy (6 kJ · mol^{-1}) shows that diffusion is the limiting part of the adsorption process. Kinetic computations establish that the initial steps of the reaction are dominated by chemical reactions and catalysis. Then,

Table 3
Parameters obtained after optimization of the rate curves with (Eq. 18). Modified Vyazovkin-Sbirrazzuoli's model (MSM). Line 1: initial values, line 2: values after optimization.

	$\ln(A_1)/s^{-1}$	$E_1/kJ{\cdot}mol^{-1}$	m	$\ln(D_0)/s^{-1}$	$E_D/kJ{\cdot}mol^{-1}$	n	K	$(S^2)/s^{-2}$[a]
1	13.00	60.00	0.00	−3.00	10.00	1.00	−4.00	$3.60 \cdot 10^{-2}$
2	18.43	73.71	0.48	10.58	40.21	0.99	−1.65	$4.36 \cdot 10^{-5}$

[a] Variance S^2.

Table 4
Parameters obtained after optimization of the rate curves with Vyazovkin-Sbirrazzuoli's model (VSM).

$\ln(A_1)/s^{-1}$	$E_1/kJ{\cdot}mol^{-1}$	$\ln(A_2)/s^{-1}$	$E_2/kJ{\cdot}mol^{-1}$	m	$\ln(D_0)/s^{-1}$	$E_D/kJ{\cdot}mol^{-1}$	n	K	$(S^2)/s^{-2}$[a]
11.62	142.59	15.72	63.07	0.57	10.59	42.44	1.06	−0.83	$3.98 \cdot 10^{-5}$

[a] Variance S^2

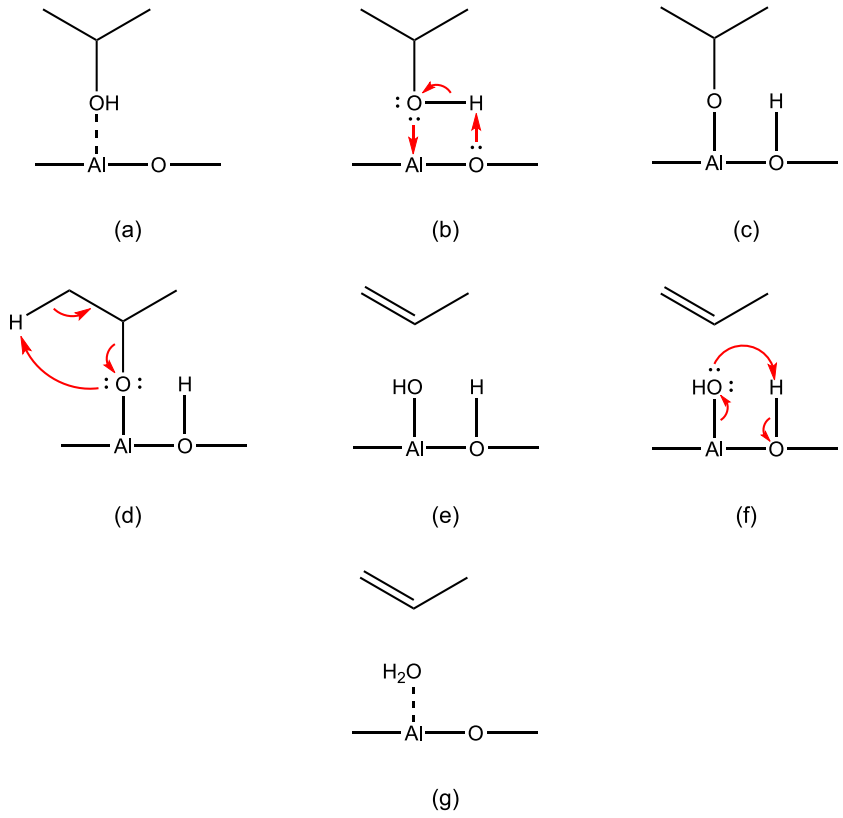

Fig. 20. E2 Reaction mechanism on acid-basic site of Al_2O_3 surface: molecular adsorbed isopropanol (a), dissociation (b), dissociated isopropanol (c), H abstraction and C − O cleavage (d), dissociated water (e), recombination (f), molecular adsorbed water (g).

the diffusion becomes rate limiting. Two models were used to highlight the E2 and E1cb mechanisms and related activated steps.

Calorimetry measurement is believed to be a powerful tool to quantify the surface strength and distribution of catalytic active sites. Combined with a pulse catalysis test, it provides direct measurements under realistic operating conditions and provides new kind of information on adsorption of reagents, desorption of products and reaction. Advanced data treatment and modelling of the calorimetric signals provide kinetic parameters that expand the understanding of the fundamental mechanisms. In this study, the technic allows for a better comprehension of the energies, kinetics and related mechanisms involved in the catalytic dehydration of isopropanol to propylene which is needed to adjust the catalyst surface and operating conditions.

CRediT authorship contribution statement

Tristan Cabanis: Writing – original draft, Visualization, Software, Methodology, Investigation, Formal analysis. **Aline Auroux:** Writing – review & editing, Conceptualization. **Jean-Luc Dubois:** Writing – review & editing. **Nicolas Sbirrazzuoli:** Writing – review & editing, Software, Formal analysis. **Georgeta Postole:** Writing – review & editing, Supervision, Project administration, Methodology, Conceptualization.

Declaration of competing interest

The authors declare that they have no known competing financial

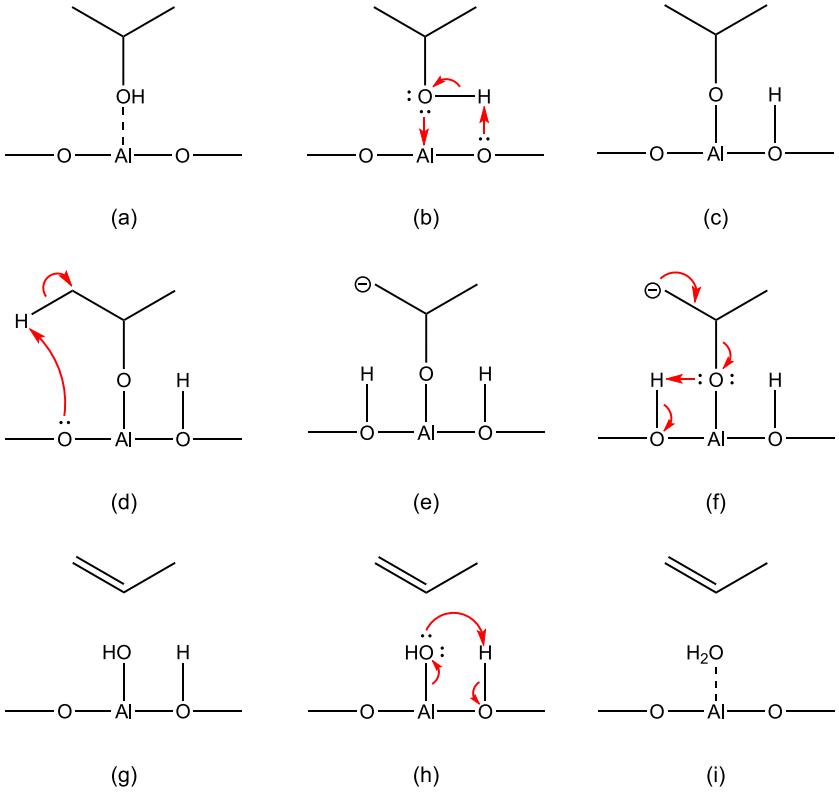

Fig. 21. $E1_{cb}$ Reaction mechanism on acid-basic site of Al_2O_3 surface: coordinated adsorbed isopropanol (a), dissociation (b), dissociated isopropanol (c), H_β abstraction (d), carbanion intermediate (e), $C_\alpha - O$ cleavage (f), dissociated water (g), recombination (h), coordinated adsorbed water (i).

interests or personal relationships that could have appeared to influence the work reported in this paper.

Acknowledgement

This work is part of PYROCO2 project that has received funding from the European Union's Horizon 2020 research and innovation programme under grant agreement No. 101037009.

Appendix A. Supplementary data

Supplementary data to this article can be found online at https://doi.org/10.1016/j.apcato.2025.207073.

Data availability

Data will be made available on request.

References

[1] G.A. Somorjai, Y. Li, Introduction to Surface Chemistry and Catalysis, 2nd ed., Wiley, Hoboken, N.J, 2010.
[2] P. Webb, Introduction to Chemical Adsorption Analytical Techniques and their Applications to Catalysis, 2003.
[3] H. Knozinger, R. Kohne, The dehydration of alcohols over alumina I. The reaction scheme, J. Catal. 5 (1966) 264–270, https://doi.org/10.1016/S0021-9517(66)80007-6.
[4] H. Knozinger, The dehydration of alcohols on alumina XIV. Reactivity and mechanism, J. Catal. 24 (1972) 57–68, https://doi.org/10.1016/0021-9517(72)90007-3.
[5] H. Knozinger, Acidic and basic properties of aluminas in relation to their properties as catalysts and supports, in: B. Imelik, C. Naccache, G. Coudurier, Y.B. Taarit, J. C. Vedrine (Eds.), Studies in Surface Science and Catalysis, Elsevier, 1985, pp. 111–125, https://doi.org/10.1016/S0167-2991(09)60161-0.
[6] E.C. DeCanio, V.P. Nero, J.W. Bruno, Identification of alcohol adsorption sites on γ-alumina, J. Catal. 135 (1992) 444–457, https://doi.org/10.1016/0021-9517(92)90046-K.
[7] A. Ouqour, G. Coudurier, J.C. Vedrine, Acid–base properties of metallic oxide catalysts studied by conversion of propan-2-ol, J. Chem. Soc. Faraday Trans. 89 (1993) 3151–3155, https://doi.org/10.1039/FT9938903151.
[8] A. Gervasini, J. Fenyvesi, A. Auroux, Study of the acidic character of modified metal oxide surfaces using the test of isopropanol decomposition, Catal. Lett. 43 (1997) 219–228, https://doi.org/10.1023/A:1018979731407.
[9] L. Österlund, Pressure gaps in heterogeneous catalysis, in: W.Y. Teoh, A. Urakawa, Y.H. Ng, P. Sit (Eds.), Heterogeneous Catalysts, 1st ed, Wiley, 2021, pp. 225–251, https://doi.org/10.1002/9783527813599.ch13.
[10] H. Topsøe, Developments in operando studies and in situ characterization of heterogeneous catalysts, J. Catal. 216 (2003) 155–164, https://doi.org/10.1016/S0021-9517(02)00133-1.
[11] A. Rodrigues, J.-M. Tatibouët, E. Fourré, Operando DRIFT spectroscopy characterization of intermediate species on catalysts surface in VOC removal from air by non-thermal plasma assisted catalysis, Plasma Chem. Plasma Process. 36 (2016) 901–915, https://doi.org/10.1007/s11090-016-9718-1.
[12] C. Rodríguez, S. Moreno, R. Molina, Operando DRIFT-MS for studying the oxidative steam reforming of ethanol (OSRE) reaction, MethodsX 10 (2023) 102169, https://doi.org/10.1016/j.mex.2023.102169.
[13] J.J. Ternero-Hidalgo, M. Daturi, G. Clet, P. Bazin, M.A. Bañares, R. Portela, M. O. Guerrero-Pérez, J. Rodríguez-Mirasol, T. Cordero, A simultaneous *operando* FTIR & Raman study of propane ODH mechanism over V-Zr-O catalysts, Catal. Today 387 (2022) 197–206, https://doi.org/10.1016/j.cattod.2021.06.012.
[14] C. Hess, New advances in using Raman spectroscopy for the characterization of catalysts and catalytic reactions, Chem. Soc. Rev. 50 (2021) 3519–3564, https://doi.org/10.1039/D0CS01059F.
[15] J.-D. Grunwaldt, A.M. Molenbroek, N.-Y. Topsøe, H. Topsøe, B.S. Clausen, *In situ* investigations of structural changes in Cu/ZnO catalysts, J. Catal. 194 (2000) 452–460, https://doi.org/10.1006/jcat.2000.2930.
[16] K. Morgan, N. Maguire, R. Fushimi, J.T. Gleaves, A. Goguet, M.P. Harold, E. V. Kondratenko, U. Menon, Y. Schuurman, G.S. Yablonsky, Forty years of temporal analysis of products, Catal. Sci. Technol. 7 (2017) 2416–2439, https://doi.org/10.1039/C7CY00678K.
[17] A.M. Efstathiou, J.T. Gleaves, G.S. Yablonsky, Transient techniques: Temporal analysis of products and steady state isotopic transient kinetic analysis, in: M. Che, J.C. Védrine (Eds.), Characterization of Solid Materials and Heterogeneous Catalysts, 1st ed., Wiley, 2012, pp. 1013–1073, https://doi.org/10.1002/9783527645329.ch22.
[18] R.J. Berger, F. Kapteijn, J.A. Moulijn, G.B. Marin, J. De Wilde, M. Olea, D. Chen, A. Holmen, L. Lietti, E. Tronconi, Y. Schuurman, Dynamic methods for catalytic kinetics, Appl. Catal. A Gen. 342 (2008) 3–28, https://doi.org/10.1016/j.apcata.2008.03.020.

[19] C. Ledesma, J. Yang, D. Chen, A. Holmen, Recent approaches in mechanistic and kinetic studies of catalytic reactions using SSITKA technique, ACS Catal. 4 (2014) 4527–4547, https://doi.org/10.1021/cs501264f.

[20] A. Auroux (Ed.), Calorimetry and Thermal Methods in Catalysis, Springer, Berlin, Heidelberg, 2013, https://doi.org/10.1007/978-3-642-11954-5.

[21] A. Auroux, Acidity and Basicity: Determination by Adsorption Microcalorimetry, in: Acidity and Basicity, Springer, Berlin, Heidelberg, 2008, pp. 45–152, https://doi.org/10.1007/3829_008.

[22] D.R. Brown, A.J. Groszek, Heats of adsorption of ammonia on a zeolite catalyst and an acid-activated clay catalyst determined by flow adsorption microcalorimetry, Langmuir 16 (2000) 4207–4212, https://doi.org/10.1021/la990897h.

[23] S.P. Felix, C. Savill-Jowitt, D.R. Brown, Base adsorption calorimetry for characterising surface acidity: a comparison between pulse flow and conventional "static" techniques, Thermochim. Acta 433 (2005) 59–65, https://doi.org/10.1016/j.tca.2005.02.012.

[24] Z. Yuan, Y. Bai, K. Gong, W. Huang, Accurate measurements of NH3 differential adsorption heat unveil structural sensitivity of Brønsted acid and Brønsted/Lewis acid synergy in zeolites, J. Phys. Chem. Lett. 15 (2024) 863–868, https://doi.org/10.1021/acs.jpclett.3c03336.

[25] R. You, Z. Li, H. Zeng, W. Huang, A flow-pulse adsorption-microcalorimetry system for studies of adsorption processes on powder catalysts, Rev. Sci. Instrum. 89 (2018) 064101, https://doi.org/10.1063/1.5024253.

[26] J. Le Bars, A. Auroux, M. Forissier, J.C. Vedrine, Active sites of V2O5/γ-Al2O3 catalysts in the oxidative dehydrogenation of ethane, J. Catal. 162 (1996) 250–259, https://doi.org/10.1006/jcat.1996.0282.

[27] J. Lin, L. Li, Y. Huang, W. Zhang, X. Wang, A. Wang, T. Zhang, In situ calorimetric study: structural effects on adsorption and catalytic performances for CO oxidation over Ir-in-CeO $_2$ and Ir-on-CeO $_2$ catalysts, J. Phys. Chem. C 115 (2011) 16509–16517, https://doi.org/10.1021/jp204288h.

[28] S. Vyazovkin, A.K. Burnham, J.M. Criado, L.A. Pérez-Maqueda, C. Popescu, N. Sbirrazzuoli, ICTAC kinetics committee recommendations for performing kinetic computations on thermal analysis data, Thermochim. Acta 520 (2011) 1–19, https://doi.org/10.1016/j.tca.2011.03.034.

[29] S. Vyazovkin, K. Chrissafis, M.L. Di Lorenzo, N. Koga, M. Pijolat, B. Roduit, N. Sbirrazzuoli, J.J. Suñol, ICTAC kinetics committee recommendations for collecting experimental thermal analysis data for kinetic computations, Thermochim. Acta 590 (2014) 1–23, https://doi.org/10.1016/j.tca.2014.05.036.

[30] H.L. Friedman, Kinetics of thermal degradation of char-forming plastics from thermogravimetry. Application to a phenolic plastic, J. Polym. Sci. C Polym. Symp. 6 (1964) 183–195, https://doi.org/10.1002/polc.5070060121.

[31] S. Vyazovkin, N. Sbirrazzuoli, Estimating the activation energy for non-isothermal crystallization of polymer melts, J. Therm. Anal. Calorim. 72 (2003) 681–686, https://doi.org/10.1023/A:1024506522878.

[32] S. Vyazovkin, N. Sbirrazzuoli, Mechanism and kinetics of epoxy−amine cure studied by differential scanning calorimetry, Macromolecules 29 (1996) 1867–1873, https://doi.org/10.1021/ma951162w.

[33] S. Vyazovkin, N. Sbirrazzuoli, Isoconversional kinetic analysis of thermally stimulated processes in polymers, Macromol. Rapid Commun. 27 (2006) 1515–1532, https://doi.org/10.1002/marc.200600404.

[34] D. Kulkarni, I.E. Wachs, Isopropanol oxidation by pure metal oxide catalysts: number of active surface sites and turnover frequencies, Appl. Catal. A Gen. 237 (2002) 121–137, https://doi.org/10.1016/S0926-860X(02)00325-3.

[35] J.-L. Dubois, G. Postole, L. Silvester, A. Auroux, Catalytic dehydration of isopropanol to propylene, Catalysts 12 (2022) 1097, https://doi.org/10.3390/catal12101097.

[36] R. Svoboda, Fraser-Suzuki function as an essential tool for mathematical modeling of crystallization in glasses, J. Eur. Ceram. Soc. 44 (2024) 401–407, https://doi.org/10.1016/j.jeurceramsoc.2023.08.050.

[37] A.C. Resentera, M.H. Rodriguez, Some limitations of the Fraser-Suzuki function for fitting thermokinetic curves, Thermochim. Acta 725 (2023) 179520, https://doi.org/10.1016/j.tca.2023.179520.

[38] S. Vyazovkin, Isoconversional Kinetics of Thermally Stimulated Processes, Springer International Publishing, Cham, 2015, https://doi.org/10.1007/978-3-319-14175-6.

[39] S. Vyazovkin, A.K. Burnham, L. Favergeon, N. Koga, E. Moukhina, L.A. Pérez-Maqueda, N. Sbirrazzuoli, ICTAC kinetics committee recommendations for analysis of multi-step kinetics, Thermochim. Acta 689 (2020) 178597, https://doi.org/10.1016/j.tca.2020.178597.

[40] N. Sbirrazzuoli, Kinetic analysis of complex chemical reactions by coupling model-free and model-fitting analysis, Thermochim. Acta 719 (2023) 179416, https://doi.org/10.1016/j.tca.2022.179416.

[41] N. Sbirrazzuoli, Interpretation and physical meaning of kinetic parameters obtained from Isoconversional kinetic analysis of polymers, Polymers 12 (2020) 1280, https://doi.org/10.3390/polym12061280.

[42] N. Sbirrazzuoli, Determination of pre-exponential factors and of the mathematical functions $f(\alpha)$ or $G(\alpha)$ that describe the reaction mechanism in a model-free way, Thermochim. Acta 564 (2013) 59–69, https://doi.org/10.1016/j.tca.2013.04.015.

[43] N. Sbirrazzuoli, Determination of pre-exponential factor and reaction mechanism in a model-free way, Thermochim. Acta 691 (2020) 178707, https://doi.org/10.1016/j.tca.2020.178707.

[44] N. Sbirrazzuoli, Advanced isoconversional kinetic analysis: insight in mechanisms and simulations. Successes and future, Thermochim. Acta 733 (2024) 179688, https://doi.org/10.1016/j.tca.2024.179688.

[45] R.-S. Zhou, R.L. Snyder, Structures and transformation mechanisms of the η, γ and θ transition aluminas, Acta Crystallogr. Sect. B: Struct. Sci. 47 (1991) 617–630, https://doi.org/10.1107/S0108768191002719.

[46] F.A.L. Dullien, Porous Media: Fluid Transport and Pore Structure, Second edition, Academic Press, San Diego New York Boston London Sydney Tokyo Toronto, 2015.

[47] J.H. de Boer, B.C. Lippens, Studies on pore systems in catalysts II. The shapes of pores in aluminum oxide systems, J. Catal. 3 (1964) 38–43, https://doi.org/10.1016/0021-9517(64)90090-9.

[48] A. Auroux, Acidity characterization by microcalorimetry and relationship with reactivity, Top. Catal. 4 (1997) 71–89, https://doi.org/10.1023/A:1019127919907.

[49] M. Zander, W. Thomas, Some thermodynamic properties of liquid ammonia: PVT data, vapor pressure, and critical temperature, J. Chem. Eng. Data 24 (1979) 1–2, https://doi.org/10.1021/je60080a003.

[50] W.F. Giauque, C.C. Stephenson, Sulfur Dioxide, The heat capacity of solid and liquid. Vapor pressure. Heat of vaporization. The entropy values from thermal and molecular data, J. Am. Chem. Soc. 60 (1938) 1389–1394, https://doi.org/10.1021/ja01273a034.

[51] A. Gervasini, A. Auroux, Thermodynamics of adsorbed molecules for a new acid-base topochemistry of alumina, J. Phys. Chem. 97 (1993) 2628–2639, https://doi.org/10.1021/j100113a026.

[52] H. Knoezinger, B. Stuebner, Adsorption of alcohols on alumina. 1. Gravimetric and infrared spectroscopic investigation, J. Phys. Chem. 82 (1978) 1526–1532, https://doi.org/10.1021/j100502a013.

[53] M. Digne, P. Sautet, P. Raybaud, P. Euzen, H. Toulhoat, Use of DFT to achieve a rational understanding of acid–basic properties of γ-alumina surfaces, J. Catal. 226 (2004) 54–68, https://doi.org/10.1016/j.jcat.2004.04.020.

[54] J.B. Peri, Infrared study of adsorption of ammonia on dry γ-Alumina1, J. Phys. Chem. 69 (1965) 231–239, https://doi.org/10.1021/j100885a034.

[55] D. Stoilova, K. Cheshkova, R. Nickolov, FTIR spectroscopy of NH3 and NO adsorption on copper-on-alumina catalysts, React. Kinet. Catal. Lett. 68 (1999) 331–337, https://doi.org/10.1007/BF02475521.

[56] K.T. Cheshkova, D.G. Stoilova, FTIR spectroscopic study of NH3 and NH3 adsorption on alumina-supported mixed copper-manganese oxide catalysts, React. Kinet. Catal. Lett. 73 (2001) 237–243, https://doi.org/10.1023/A:1014190703421.

[57] M.E. Van Leeuwen, Derivation of Stockmayer potential parameters for polar fluids, Fluid Phase Equilib. 99 (1994) 1–18, https://doi.org/10.1016/0378-3812(94)80018-9.

[58] B. Fubini, V. Bolis, M. Bailes, F.S. Stone, The reactivity of oxides with water vapor, Solid State Ionics 32–33 (1989) 258–272, https://doi.org/10.1016/0167-2738(89)90230-0.

[59] G. Busca, P.F. Rossi, V. Lorenzelli, M. Benaissa, J. Travert, J.C. Lavalley, Microcalorimetric and Fourier transform infrared spectroscopic studies of methanol adsorption on alumina, J. Phys. Chem. 89 (1985) 5433–5439, https://doi.org/10.1021/j100271a024.

[60] R.M. Stephenson, S. Malanowski, Handbook of the Thermodynamics of Organic Compounds, Springer Netherlands, Dordrecht, 1987, https://doi.org/10.1007/978-94-009-3173-2.

[61] H. Knözinger, Dehydration of alcohols on aluminum oxide, Angew. Chem. Int. Ed. Eng. 7 (1968) 791–805, https://doi.org/10.1002/anie.196807911.

[62] A.V. Deo, I.G. Dalla Lana, Infrared study of the adsorption and mechanism of surface reactions of 1-propanol on γ-alumina and γ-alumina doped with sodium hydroxide and chromium oxide, J. Phys. Chem. 73 (1969) 716–723, https://doi.org/10.1021/j100723a038.

[63] A.V. Deo, T.-T. Chuang, I.G. Dalla Lana, Infrared studies of adsorption and surface reactions of some secondary alcohols, C3 to C5, on γ-alumina and γ-alumina doped with sodium hydroxide, J. Phys. Chem. 75 (1971) 234–239, https://doi.org/10.1021/j100672a009.

[64] K. Larmier, C. Chizallet, N. Cadran, S. Maury, J. Abboud, A.-F. Lamic-Humblot, E. Marceau, H. Lauron-Pernot, Mechanistic investigation of isopropanol conversion on alumina catalysts: location of active sites for alkene/ether production, ACS Catal. 5 (2015) 4423–4437, https://doi.org/10.1021/acscatal.5b00723.

[65] G. Feng, C.-F. Huo, C.-M. Deng, L. Huang, Y.-W. Li, J. Wang, H. Jiao, Isopropanol adsorption on γ-Al2O3 surfaces: a computational study, J. Mol. Catal. A Chem. 304 (2009) 58–64, https://doi.org/10.1016/j.molcata.2009.01.024.

[66] R.L. Gale, J. Haber, F.S. Stone, Adsorption calorimetry on granulated catalysts. A study of adsorption processes relating to isopropanol dehydrogenation, J. Catal. 1 (1962) 32–38, https://doi.org/10.1016/0021-9517(62)90006-4.

[67] M.E. Dry, R.A. Beebe, Adsorption studies on bone mineral and synthetic hydroxyapatite, J. Phys. Chem. 64 (1960) 1300–1304, https://doi.org/10.1021/j100838a042.

[68] V. Moravek, M. Kraus, Transient behavior of the system ethanol-diethyl ether-water-alumina, J. Catal. 87 (1984) 452–460, https://doi.org/10.1016/0021-9517(84)90205-7.

[69] N.A. Lange, Lange's Handbook of Chemistry, 15. ed, McGraw-Hill, New York, NY, 1999.

[70] J.D. de Casquero Ruiz, J.M. Guil Pinto, A. Pérez Masiá, A. Ruiz Paniego, Thermodynamics of the adsorption of hydrocarbons on alumina, J. Chem. Thermodyn. 18 (1986) 903–914, https://doi.org/10.1016/0021-9614(86)90148-5.

[71] V. Majer, V. Svoboda, Enthalpies of vaporization of organic compounds: A critical review and data compilation, 1986. https://www.osti.gov/etdeweb/biblio/6190977 (accessed May 7, 2025).

[72] P.F. Rossi, G. Oliveri, M. Bassoli, Heat of water chemisorption on α-Al2O3 at 200–400 °C, J. Chem. Soc. Faraday Trans. 90 (1994) 363–367, https://doi.org/10.1039/FT9949000363.

[73] R.L. Gibson, M.J.H. Simmons, E. Hugh Stitt, J. West, S.K. Wilkinson, R.W. Gallen, Kinetic modelling of thermal processes using a modified Sestak-Berggren equation, Chem. Eng. J. 408 (2021) 127318, https://doi.org/10.1016/j.cej.2020.127318.
[74] M.E. Davis, R.J. Davis, Fundamentals of Chemical Reaction Engineering, International ed, McGraw-Hill, Boston, 2003.
[75] N. Sbirrazzuoli, S. Vyazovkin, Two step model for crosslinking polymerization with account of diffusion, Chem. Eng. J. 481 (2024) 148414, https://doi.org/10.1016/j.cej.2023.148414.